



## Climate change and hydrological dam safety: a stochastic methodology based on climate projections

Marco Lompi, Luis Mediero, Enrique Soriano & Enrica Caporali

To cite this article: Marco Lompi, Luis Mediero, Enrique Soriano & Enrica Caporali (2023) Climate change and hydrological dam safety: a stochastic methodology based on climate projections, Hydrological Sciences Journal, 68:6, 745-763, DOI: [10.1080/02626667.2023.2192873](https://doi.org/10.1080/02626667.2023.2192873)

To link to this article: <https://doi.org/10.1080/02626667.2023.2192873>



© 2023 The Author(s). Published by Informa UK Limited, trading as Taylor & Francis Group.



Published online: 03 May 2023.



Submit your article to this journal [↗](#)



Article views: 336





View related articles [↗](#)



View Crossmark data [↗](#)

# Climate change and hydrological dam safety: a stochastic methodology based on climate projections

Marco Lompi <sup>a,b</sup>, Luis Mediero <sup>b</sup>, Enrique Soriano <sup>b</sup> and Enrica Caporali <sup>a</sup>

<sup>a</sup>Department of Civil and Environmental Engineering, University of Florence, Florence, Italy; <sup>b</sup>Department of Civil Engineering: Hydraulics, Energy and Environment, Universidad Politécnica de Madrid, Madrid, Spain

## ABSTRACT

Climate change will likely increase the frequency and magnitude of extreme precipitation events and floods, increasing design peak flows that could lead to underestimates in current spillway capacity. Therefore, new methodologies for hydrological dam safety assessment considering climate change are required. This study presents a methodology that considers the impact of climate change on both inflow hydrographs and initial reservoir water levels. Moreover, the uncertainty in the procedure is assessed. The methodology is applied to the Eugui Dam in the River Arga catchment (Spain). An ensemble of 12 climate models is used. The results show an increase in the maximum reservoir water level during flood events and in the overtopping probability in the Representative Concentration Pathway 8.5 (RCP 8.5 scenario), especially in the 2071–2100 time window. The proposed methodology can be useful to assess future hydrological dam safety, fulfilling the requirements of recent regulations to consider the impact of climate change on dams.

## ARTICLE HISTORY

Received 6 April 2022  
Accepted 6 February 2023

## EDITOR

A. Castellarin

## GUEST EDITOR

E. Volpi

## KEYWORDS

climate change; hydrological dam safety; floods; overtopping; uncertainty assessment; stochastic procedure

## 1 Introduction

It is widely recognized that climate change will impact the hydrological cycle. A warmer climate increases the frequency and intensity of extreme precipitations (Donat *et al.* 2016, Li *et al.* 2019, Myhre *et al.* 2019), enhancing flood hazards. Floods are the leading cause of natural disaster deaths worldwide, with more than half a million fatalities caused by rain-induced floods in the period 1980–2009 (Doocy *et al.* 2013). Therefore, the impacts of future climate conditions on flood risks should be assessed to develop plan adaptation strategies that consider extreme event risks (IPCC 2012, 2014). In addition, floods represent the hydrological load on dams. Therefore, changes in climatic conditions will likely affect hydrological dam safety (Bowles *et al.* 2013).

The impact of climate change on floods can be studied using either trend analyses of streamflow data recorded in the last few decades or rainfall–runoff modelling with climate projections as input data (Quintero *et al.* 2018). Rainfall and temperature climate projections are generated by global climate models (GCM), based on a set of greenhouse emission scenarios in the future called Representative Concentration Pathways (RCPs) (Meinshausen *et al.* 2011). RCPs 4.5 and 8.5 are usually considered to assess the impact of climate change on floods (Kim *et al.* 2013, Babur *et al.* 2016, Nilawar and Waikar 2019, Marahatta *et al.* 2021, Oubennaceur *et al.* 2021). RCP 4.5 assumes that the peak of emissions occurs around 2040, declining with their stabilization at the end of

the century (Thomson *et al.* 2011); RCP 8.5 considers that the radiative forcing will increase throughout the century (Riahi *et al.* 2011). However, the spatial resolution of GCM outputs is usually coarse for hydrological and impact assessment studies at the catchment scale. Therefore, GCM outputs are refined in a smaller domain with downscaling techniques, such as regional climate models (RCMs).

Global studies on the impact of climate change on floods have shown significant increasing trends in the annual median of flood durations (Najibi and Devineni 2018). A general increase in flood damages in the largest rivers in the world was detected for the time window 2080 in RCP 8.5 (Winsemius *et al.* 2015). A similar pattern is recognized by Alfieri *et al.* (2015); they found a general increase in the 100-year flood in Europe for RCP 8.5. On the contrary, other studies point to a decrease in flood frequency, especially in southern and eastern Europe (Hirabayashi *et al.* 2013, Blöschl *et al.* 2019, Brunner *et al.* 2019).

However, a clear pattern of the expected changes in future hydraulic risks in southern Europe cannot be identified. Discrepant results can be found as studies usually consider different sets of climate models, downscaling techniques, or bias correction methods (Kundzewicz *et al.* 2017). For example, while Dankers and Feyen (2008) and Rojas *et al.* (2012) found a decrease in the future 100-year flood in Spain, Roudier *et al.* (2016) detected an increasing trend.

Despite the fact that a clear signal of change is not evident, stationarity will no longer be appropriate for long-term dam

safety management (USACE 2016). Moreover, many large dams were designed for downstream flood-control purposes at the time of their construction (Chen and Hossain 2019). However, downstream urban areas may have expanded, or safety regulations may have changed from that time. Therefore, several studies have proposed methodologies to assess dam safety in the future considering climate change projections. Fluixá-Sanmartín *et al.* (2019b) found a significant uncertainty in the risk given by climate projection inputs for RCP 8.5, while an increase in both social and economic risks is detected for the RCP 4.5 scenario. Lee and You (2013) combined the effect of climate change with a reduction of the reservoir flood control volume caused by sedimentation, concluding that the major source of risk in the future was the magnitude of extreme events. Several aspects are related to dam safety. Indeed, both climatic and non-climatic drivers can generate dam failures, such as overtopping, piping, or sliding, and several methodologies have been developed to describe these phenomena (Wahl 2004, Froehlich 2008, Ahmadisharaf *et al.* 2016, Peter *et al.* 2018).

This study focuses on hydrological dam safety and overtopping hazard. Overtopping occurs when the reservoir water level exceeds the dam crest elevation, spilling over the downstream dam face. Over the last century, almost 30% of all dam failures worldwide were caused by overtopping (Jandora *et al.* 2008), and floods represent their main driver (Costa 1985). A detailed analysis of overtopping hazards requires comprehensive information on hydrology, hydraulics, characteristics of the dam and the use of routing methods (Michailidi and Bacchi 2017). Therefore, catchment-scale studies are required to properly assess the impact of climate change on future dam safety, although more tools are available to assess overtopping probabilities in dams at the regional scale (Fluixá-Sanmartín *et al.* 2019a). In addition, Fluixá-Sanmartín *et al.* (2018) state that most studies tend to focus only on the assessment of the expected changes in the future hydrological loads (Bahls and Holman 2014, Chernet *et al.* 2014, Novembre *et al.* 2015), such as changes in inflow hydrographs, neglecting other important aspects, such as future variations in initial reservoir water levels. Indeed, climate change is expected to affect future water availability because of increasing precipitation temporal variability, decreasing precipitation magnitudes, and increasing potential evapotranspiration (IPCC 2014). Changes in the overtopping probability can be detected with trend analysis and hydrological modelling of observed data (Ahmadisharaf and Kalyanapu 2015). This study, by contrast, provides a methodology to estimate the expected changes in dam overtopping based on climate projections.

Dam risk analysis is usually linked to high return-period floods, although such estimates involve great uncertainty. Therefore, the assessment of uncertainty due to hydrological and climate modelling should be accounted for to provide helpful information for decision making (Prudhomme and Davies 2009). This study presents a methodology that considers the impact of climate change on both floods and reservoir water levels to assess hydrological dam safety. Moreover, a stochastic approach that considers all the sources of uncertainty in the procedure is developed. The methodology is applied to the Eugui Dam in the River Arga (Spain), with a catchment area of 69 km<sup>2</sup>.

Section 2 describes the data and case study. Section 3 presents the methodology used to assess the impact of climate change on hydrological dam safety and a description of the models used in the analysis. Section 4 gives the results regarding the future reservoir water levels and peak inflows, as well as the changes in maximum reservoir water levels and the overtopping probability after the incorporation of the uncertainty. Finally, the discussion (Section 5) and conclusion (Section 6) are included.

## 2 Data and case study

### 2.1 Case study: Arga River and Eugui Dam

The methodology is applied to the Eugui Dam in the Arga River catchment in northern Spain (Fig. 1). The Arga River crosses the city of Pamplona and has a catchment area of 2759 km<sup>2</sup>. While the drainage area to the city of Pamplona is 510 km<sup>2</sup>, the catchment area of the Eugui reservoir is 69 km<sup>2</sup> (Figs 1(b) and 2(a)). The main purpose of the dam is to supply water for the downstream population, but it is also used for hydropower generation. The Eugui Dam has a gated spillway (Fig. 2(b)) with its crest elevation at 625 m a.s.l. The conservation pool has a storage capacity of 21.8 million m<sup>3</sup> and its top elevation is at 628 m a.s.l. The spillway capacity is 270 m<sup>3</sup>/s at the top of the flood control pool. The dam crest is at 630 m a.s.l with a length of 252 m. Lompi *et al.* (2021) quantified changes in the design floods by focusing on flood hazards in the city of Pamplona. Such results are also available at the Eugui Dam, as the Real-time Interactive Basin Simulator (RIBS) model (Section 3.1) is fully distributed.

### 2.2 Data

The observed data consist of precipitation, temperature, water levels (or storage volumes) at the reservoir, and outflow discharges released by the dam outlets (Table 1). Two sources of data on reservoir water levels are available. Daily data are available for 40 years (1978–2018) at the E9825 gauging site, while data at a 15-min time resolution are available for 23 years (1998–2021) at the E025 gauging site.

The analysis of the observed data is made to identify the empirical reservoir water level frequency, i.e. the probability associated with a given pool level inside the reservoir in the current scenario, and to obtain the inflow peak discharges. This information is used to assess the hydrological dam safety in the current scenario. Moreover, observed data are used to calibrate the hydrological models (RIBS and Hydrologiska Byråns Vattenbalansavdelning (HBV)) described in the next sections. Inflow discharges in the reservoir were obtained through a mass balance with outflow discharges (A152) and storage volumes (E025). The Annual Maxima Series (AMS) of daily inflow discharges is obtained for the period 1978–2021. In addition, AMS of 15-min inflow discharges is extracted in the period 1998–2021. The peaks of the hydrograph with a 15-min resolution in the period 1978–1997 are estimated from daily data. In particular, a linear regression is fitted to the couples of daily discharge and 15-min peaks obtained in the last part of the time series (1998–2021) with a peak over threshold (POT3), i.e. considering three events each year on average. A generalized extreme value distribution (GEV) is fitted to the AMS of inflow

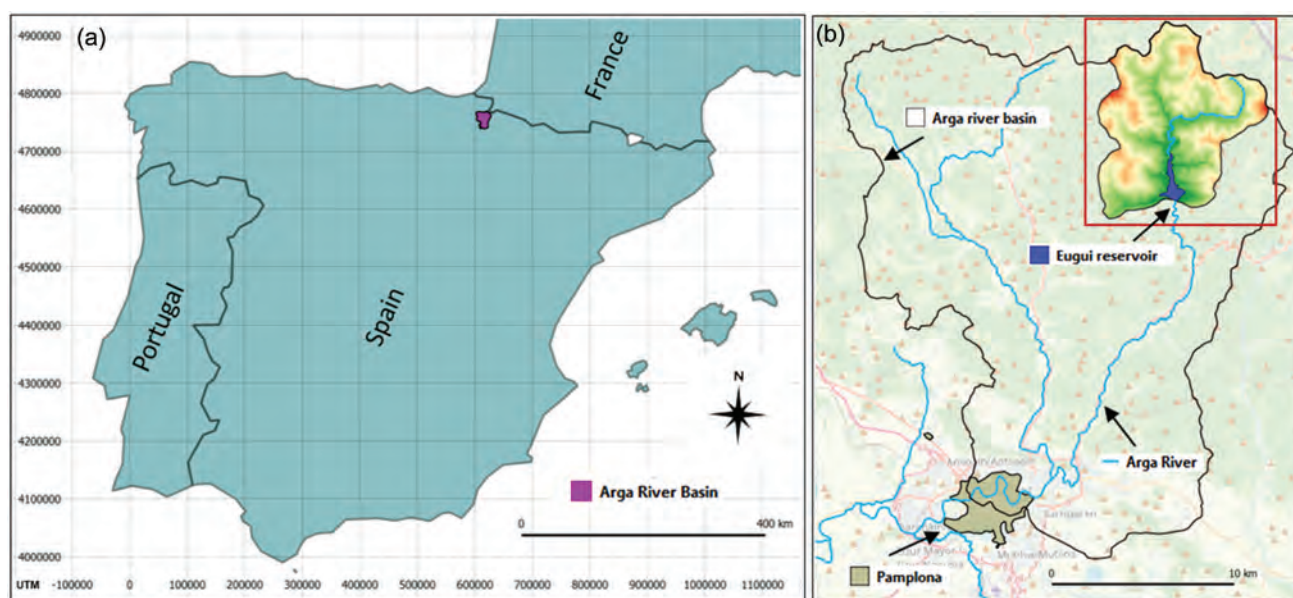


**Figure 1.** (a) Location of the Arga River basin, upstream of the city of Pamplona in northern Spain; and (b) location of the Eugui Reservoir within the catchment.

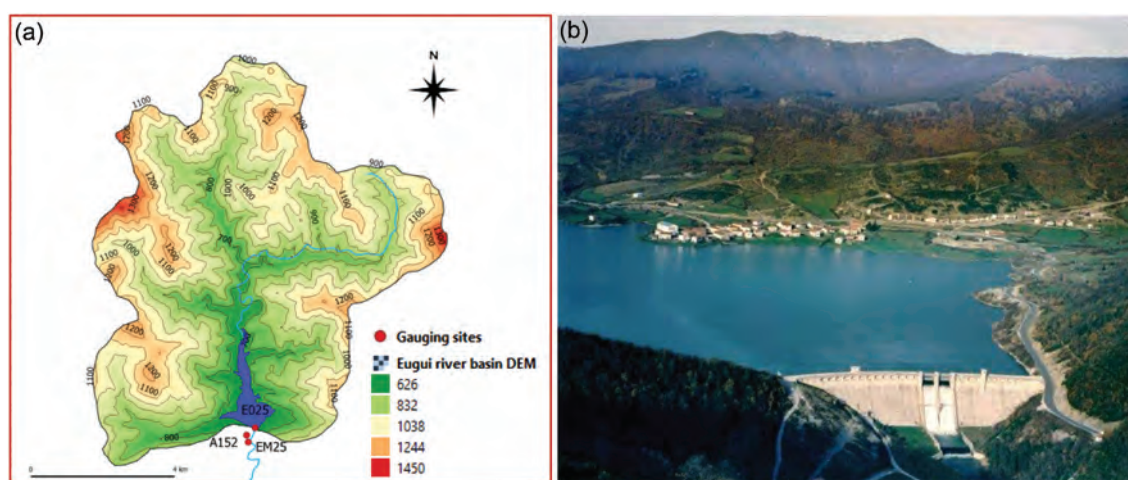


**Figure 2.** (a) Arga River catchment upstream of the Eugui reservoir in northern Spain, with gauging site location and digital elevation model; and (b) Eugui Dam and reservoir (source: <https://www.iagua.es/data/infraestructuras/presas/eugui>). E9825 and EA025 gauging sites have the same location. Therefore, only the position of the newest instrument is shown in Fig. 2(a).

**Table 1.** Observed data used in the study.

Name	Measured variable	Period	Time resolution
E9825	Reservoir water level	1978–2018	Daily
E025	Reservoir water level	1998–2021	15 min
A152	Outflow discharge	1998–2021	15 min
EM25	Rainfall and temperature	2008–2021	15 min

discharges to analyse the dam hydrological load in the current scenario, as homogeneous regions are identified in Spain at the national scale by the Centre for Hydrographic Studies of CEDEX (Centro de Estudios y Experimentación de Obras Públicas, in Spanish), and a given probability distribution function is recommended in each region (Jiménez-Álvarez *et al.* 2013). The POT approach could be preferred for the definition of the design rainfalls (Bezak *et al.* 2014), as AMS either can contain small events in years with no significant storms, or cannot consider important events lower than the annual

maximum because several extremes events occurred in the same year. Nevertheless, the selection of the threshold and the transformation of the POT frequency curve into an AMS frequency curve represent additional sources of uncertainty. Therefore, the AMS approach has been selected in this study.

The climate change data consist of rainfall and temperature projections in the period 2006–2100 supplied by 12 climate models of the EURO-CORDEX (Jacob *et al.* 2020), considering two emission scenarios (RCP 4.5 and RCP 8.5) (Table 2). The use of rainfall projections is described in the Methodology section.

### 3 Methodology

Methodologies intended to assess the impact of climate change on hydrological dam safety should estimate the expected

**Table 2.** Ensemble of the 12 climate models of the EURO-CORDEX considered in the analysis.

Code	Abbreviation	GCM	RCM
1	ICH-CCL	ICHEC-EC-EARTH	CLMcom-CCLM4-8-17
2	MPI-CCL	MPI-ESM-LR	CLMcom-CCLM4-8-17
3	MOH-RAC	MOHC-HadGEM2-ES	KNMI-RACMO22E
4	CNR-RAC	CNRM-CERFACS-CM5	CLMcom-CCLM4-8-17
5	ICH-RAC	ICHEC-EC-EARTH	KNMI-RACMO22E
6	MOH-CCL	MOHC-HadGEM2-ES	CLMcom-CCLM4-8-17
7	IPS-WRF	IPSL-CM5A-MR	IPSL-WRF331F
8	IPS-RCA	IPSL-CM5A-MR	SMHI-RCA4
9	MOH-RCA	MOHC-HadGEM2-ES	SMHI-RCA4
10	ICH-RCA	ICHEC-EC-EARTH	SMHI-RCA4
11	CNR-RCA	CNRM-CERFACS-CM5	SMHI-RCA4
12	MPI-RCA	MPI-ESM-LR	SMHI-RCA4

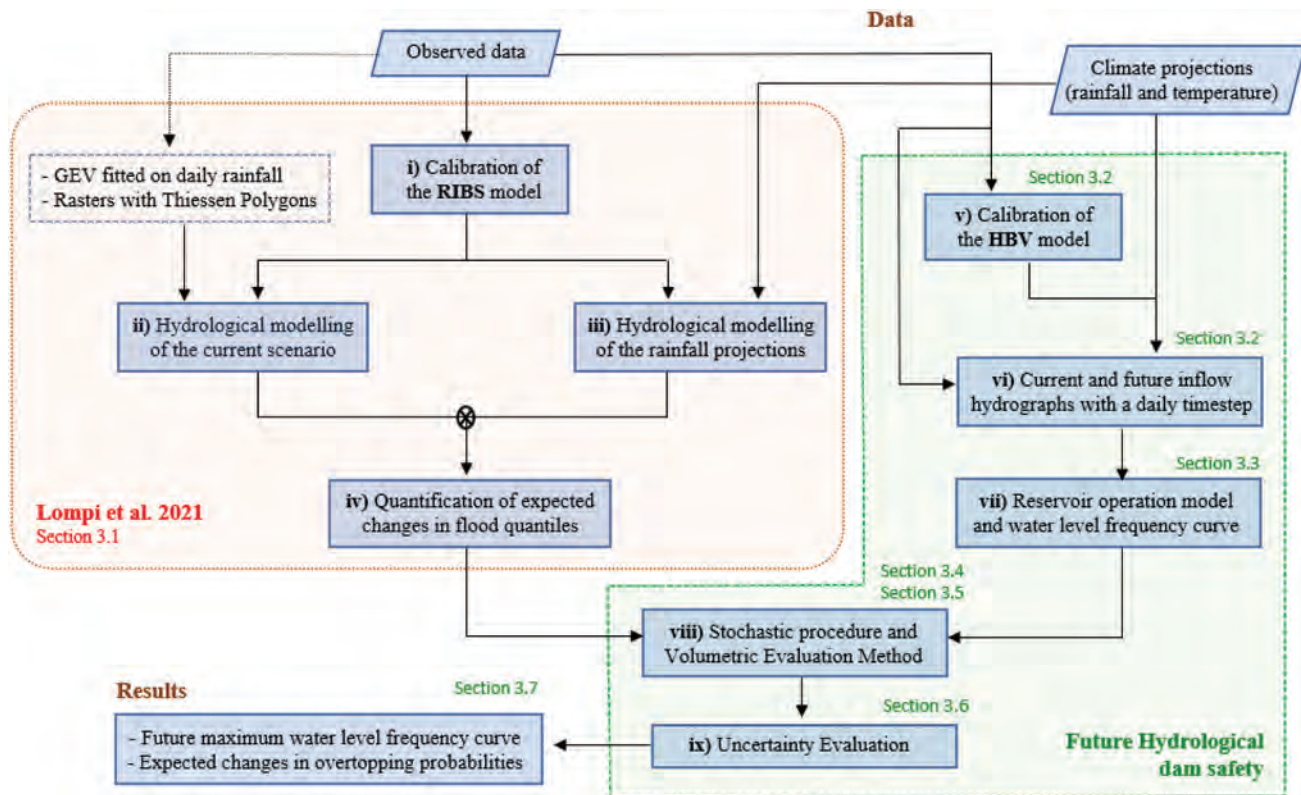
changes in flood quantiles and assess the impact of climate change on the reservoir water level frequency. The choice of the most appropriate hydrological model depends on the spatial and temporal scale of the phenomenon to be represented. For this reason, the fully distributed event-based hydrological model RIBS (Section 3.1) is chosen to describe the flooding process in the river basin associated with high rainfall quantiles, as it has a fine spatial and temporal scale (sub-daily). On the other hand, the continuous model HBV (Section 3.2) has a too coarse temporal scale to describe the flooding process in a small catchment, but it is suitable to evaluate the expected changes in reservoir water levels with long-term simulation. An overview of the methodology is summarized in Fig. 3, in which all the further subsections are shown.

The impact of climate change on floods in the River Arga catchment is quantified using the expected delta changes in precipitation quantiles extracted from climate projections in Spain (Garijo and Mediero 2019). The RIBS distributed

hydrological model is used to quantify the expected changes in flood quantiles at the Eugui Dam (Lompi *et al.* 2021) (Section 3.1).

The HBV continuous hydrological model is used with a daily time step to simulate inflow discharges at the Eugui reservoir, considering rainfall and temperature climate change projections as input data. HBV can simulate in shorter computation times the long time series of daily inflows at the reservoir. The HBV model is calibrated and utilized to simulate the catchment daily runoff response using climate projections as input data (Section 3.2). A reservoir simulation model that considers reservoir operation rules is developed to obtain daily reservoir water levels using daily inflow discharges supplied by the HBV model as input data (Section 3.3). Expected changes in reservoir water levels in the future are obtained.

A stochastic procedure is developed to obtain both the maximum reservoir water level frequency and the maximum outflow discharge released from the dam

**Figure 3.** Flowchart of the methodology used to assess the impact of climate change on the future hydrological dam safety.

(Section 3.4). The volumetric evaluation method (VEM) is used to simulate flow routing processes in the reservoir during flood events, as the Eugui Dam has a gated spillway (Girón 1988). Random inflow hydrographs and random initial water levels are combined in VEM (Section 3.5). The frequency curve of maximum reservoir water levels is obtained for each scenario, assessing the expected changes in the exceedance probability of dam overtopping. Moreover, the sources of uncertainty in the methodology are quantified (Section 3.6). The results are presented with overtopping probabilities and expected delta changes in maximum reservoir water levels (Section 3.7).

### 3.1 RIBS model: description, calibration and quantification of the expected change in flood quantiles

This section briefly describes the RIBS model and the work done by Lompi *et al.* (2021), where more information can be found on how the Real-time Interactive Basin Simulator (RIBS) has been calibrated and used to assess expected changes in inflow hydrographs at the Eugui Dam. The methodology is based on a comparison of flood quantiles in the current scenario with those in future periods.

RIBS is an event-based distributed hydrological rainfall-runoff model that extracts the required information for the catchment from a digital elevation model (DEM). RIBS uses the Brooks-Corey equation to estimate rainfall losses and runoff in each cell (Cabral *et al.* 1992). Then, runoff is propagated in the domain considering hillslope and reach velocities. Hydrograph shapes (volume) and peaks depend on the soil hydraulic conductivity and the two velocities, which are evaluated through several model parameters that must be calibrated. More information about the RIBS model and its calibration can be found in Mediero *et al.* (2011) and Garrote and Bras (1995a, 1995b).

RIBS was calibrated in the Arga catchment by comparing a set of observed and modelled hydrographs identified with a POT analysis using a hydrometer located in Pamplona. Daily rainfall data were used to estimate design rainfalls in the current scenarios with a GEV distribution. Expected delta changes in daily precipitation quantiles in the future were extracted from rainfall climate projections supplied by 12 combinations of GCMs and RCMs (Table 2) of the EURO-CORDEX Program by Garijo and Mediero (2019). Since the position of the grid of the delta changes differs from the raingauge locations, the future design rainfall field is obtained in each scenario combining the raster of the design hyetographs in the current scenario with the raster of the delta changes. The rasters are obtained with the Thiessen polygon technique. Delta changes in peak flow quantiles were estimated for seven return periods (2, 5, 10, 50, 100, 500 and 1000 years), two RCPs (RCP 4.5 and RCP 8.5) and three future time windows (2011–2040, 2041–2070, 2071–2100) (Lompi *et al.* 2021).

### 3.2 HBV model: description, calibration and hydrological modelling of the climate change scenarios

Hydrologiska Byråns Vattenbalansavdelning (HBV) is a semi-distributed conceptual continuous rainfall-runoff model

(Bergström 1976, 1992). In this model, a catchment is divided into sub-catchments, which can be further divided into a set of elevation and vegetation zones. The data required by the model are daily temperature, precipitation, and potential evapotranspiration ( $PET$ ), which must be calculated externally to the model. The model structure is divided into three modules (snow and glacier routine, soil routine, and response function routine). In the snow routine, precipitation is converted into snow accumulation with a snowfall correction factor ( $SFCF$ ) when the temperature is under the temperature threshold ( $TT$ ).  $CFMAX$  represents the equivalent melted snow as a function of the difference between the actual temperature and  $TT$ .

The infiltrated water fills the soil box, recharging the groundwater depending on the ratio between its current content ( $SM$ ) and its largest possible value ( $FC$ ). The soil is characterized by two reservoirs. The maximum percolation rate ( $PERC$ ) defines the underground flow between the two reservoirs.  $BETA$  determines the relative contribution to runoff from rain or snowmelt. In the soil routine, when the soil moisture is above a given threshold ( $LP*FC$ ), evapotranspiration ( $AET$ ) is equal to  $PET$ . Otherwise,  $AET$  is reduced linearly from its maximum value ( $PET$ ) to zero. Runoff from the groundwater is simulated as a release from linear reservoirs with parameters  $K0$ ,  $K1$  and  $K2$  depending on whether the upper groundwater box is above a threshold,  $UZL$ , or not. The response routing determines the discharge using a triangular weighting function characterized by the parameter  $MAXBAS$  (Seibert and Vis 2012). In this study, the HBV-light software has been used.

First,  $PET$  is calculated from temperature projections, using the Hargreaves equation (Equation 1) (Hargreaves 1981, Hargreaves and Samani 1985). In the current scenario, all the data required by the Penman-Monteith equation (Monteith 1965) are available, although climate change data do not include humidity and wind speed projections. Therefore, the Hargreaves equation is also used to calibrate the HBV model in the current scenario:

$$PET = 0.0022 \cdot R_A \cdot \delta_T^{0.5} \cdot (T + 17.8) \quad (1)$$

where  $R_A$  is the mean extraterrestrial radiation, which depends on the latitude of the case study;  $\delta_T$  is the difference between the mean monthly maximum temperature and the mean monthly minimum temperature; and  $T$  is the daily temperature.

The HBV model is calibrated using Monte Carlo simulations with a single objective function to evaluate model errors: the efficiency of the model ( $R_{eff}$ ). This is how the HBV-light model refers to the Nash-Sutcliffe model efficiency  $NSE$  (Nash and Sutcliffe 1970) (Equation 2). Eleven parameters are considered for each vegetation zone ( $TT$ ,  $CFMAX$ ,  $FC$ ,  $LP$ ,  $BETA$ ,  $PERC$ ,  $UZL$ ,  $K0$ ,  $K1$ ,  $K2$ ,  $MAXBAS$ ), the values of which are varied within given ranges, to find the optimal combination for the case study.

$$R_{eff} = NSE = 1 - \frac{\sum (Q_{sim}(i) - Q_{obs}(i))^2}{\sum (Q_{obs}(i) - \overline{Q_{obs}})^2} \quad (2)$$

where  $Q_{sim}(i)$  is the simulated discharge at the  $i$ th day;  $Q_{obs}(i)$  is the mean daily observed discharge at the  $i$ th day, and  $\overline{Q_{obs}}$  is

the mean value of the observed daily discharge time series. The optimum value of  $R_{eff}$  is one when there is no bias between simulations and observations. The calibration target in this study consists of obtaining an  $R_{eff}$  value of at least 0.85, as model evaluation guidelines (table 8 in Moriasi *et al.* 2015) considered 0.8 as the threshold to reach a *very good* performance rating in estimating flow at the river basin scale with a daily time step. Moreover, the last part of the observation time series is used for the independent validation of the HBV model. The model evaluation metrics used to describe the HBV model performance after its calibration (in the calibration and validation period) are: the *NSE* ( $R_{eff}$ ), the root mean squared error (*RMSE*)-observations standard deviation ratio (*RSR*) (Equation 3) and the percent bias (*PBIAS*) (Equation 4), to refer to Moriasi *et al.* (2015).

$$RSR = \frac{RMSE}{STDEV_{obs}} = \frac{\sqrt{\sum (Q_{sim}(i) - Q_{obs}(i))^2}}{\sqrt{\sum (Q_{obs}(i) - \overline{Q_{obs}})^2}} = \sqrt{1 - NSE} \quad (3)$$

$$PBIAS = \frac{\sum (Q_{sim}(i) - Q_{obs}(i)) * 100}{\sum Q_{obs}(i)} \quad (4)$$

The HBV model is calibrated with the available rainfall and temperature data at the gauging site EM25 (Table 1) over a period of 13 years from January 2008 to May 2021 and validated in the last year of data, from June 2021 to July 2022. Climate projections of rainfall, temperature and *PET* in the period 2006–2100 are used in the calibrated HBV model as input data, to obtain future inflow discharge time series in the reservoir with a daily time step ( $Q_{in,i}$ ). However, the first four years are skipped for the sake of model stabilization. Therefore, the time series obtained in the period 2010–2100 are used as input data for the reservoir operation model (Section 3.3) to obtain daily reservoir water levels at the Eugui Dam.

### 3.3 Reservoir operation model

A reservoir operation model has been developed to simulate dam operations, in order to obtain the expected daily time series of reservoir water levels in the future. Daily outflow discharges ( $Q_{out,D}$ ) released by spillways and outlet works depend on dam operations, such as environmental flows released to sustain ecosystems in the downstream river; water supply to meet municipal, industrial and agricultural water demands; and flood control operations to minimize downstream flooding. The Eugui Dam has an outlet work composed of two closed pipelines and a gated spillway with a crest length of 25 m. The maximum outflow discharge that can be released by both outlet works and spillway at a given time step  $i$  ( $Q_{max,i}$ ) depends on the reservoir water level at the time step  $i$  ( $WL_i$ ). Maximum daily water releases by the spillway in a given time step ( $Q_{spill,i}$ ) are assumed to equal the inflow water volume that cannot be stored in the reservoir.  $Q_{max,i}$  will be equal to the sum of the releases from both the outlet works and the spillway when  $WL_i$  is greater than the elevation of the spillway gate upper limb ( $h_{gate}$ ).  $Q_{max,i}$  will be equal to the maximum release by the outlet works,

considering that they are completely open, when  $WL_i$  is between the elevation of the outlet work inlet ( $h_{outlet}$ ) and  $h_{gate}$ .  $Q_{max,i}$  is equal to zero when  $WL_i$  is below  $h_{outlet}$ .

$$\begin{cases} Q_{max,i} = A_{outlet} \sqrt{\frac{2g(WL_i - h_{outlet})}{1.5 + \frac{\lambda_i L_{outlet}}{D_{outlet}}}} + Q_{spill,i} & \text{if } WL_i > h_{gate} \\ Q_{max,i} = A_{outlet} \sqrt{\frac{2g(WL_i - h_{outlet})}{1.5 + \frac{\lambda_i L_{outlet}}{D_{outlet}}}} & \text{if } h_{outlet} < WL_i \leq h_{gate} \\ Q_{max,i} = 0 & \text{if } WL_i \leq h_{outlet} \end{cases} \quad (5)$$

where  $A_{outlet}$ ,  $L_{outlet}$ ,  $D_{outlet}$ , and  $h_{outlet}$  are the area, length, diameter and intake elevation of the outlet work, respectively;  $\lambda_i$  is the Darcy friction coefficient at the time step  $i$  that considers the energy loss in a closed pipe (obtained in this study with the Colebrook-White equation); the coefficient 1.5 considers the energy loss at both the intake and outtake of the closed conduit; and  $Q_{spill,i}$  is the maximum discharge the spillway can release at the time step  $i$ . The outflow discharge at the day  $i$  ( $Q_{out,i}$ ) will be equal or smaller than  $Q_{max,i}$  (Equation 5) and is obtained as:

$$\begin{cases} Q_{out,i} = \alpha_m \cdot EF_m + K(\beta_m \cdot Q_{in,i} + \gamma_m) & \alpha_m > 1; Q_{out,i} < Q_{max,i} \\ Q_{out,i} = Q_{max,i} & Q_{out,i} \geq Q_{max,i} \end{cases} \quad (6)$$

where  $EF_m$  is the environmental flow in the  $m$ th month;  $Q_{in,i}$  is the daily inflow discharge in the reservoir at day  $i$ ;  $\alpha_m$ ,  $\beta_m$ ,  $\gamma_m$  are three parameters for each month of the year ( $m = 1, \dots, 12$ ) that are used to calibrate the reservoir operation model; and  $K$  is a parameter that considers the flood control process in the reservoir at the most extreme events. In particular, when  $WL_i$  is below the maximum reservoir water level,  $K$  is 0 and  $Q_{out,i}$  only depends on  $EF_m$ . When  $WL_i$  is close to the maximum reservoir water level,  $K$  equals 1 and  $Q_{out,i}$  also depends on  $Q_{in,i}$  to consider outflow releases by the spillway. In addition, if  $Q_{out,i}$  exceeds  $Q_{max,i}$  in a given time step,  $Q_{out,i}$  will be equal to  $Q_{max,i}$ , as the reservoir cannot release  $Q_{out,i}$  at that time step given the reservoir water level  $WL_i$ .

In the reservoir operation model,  $Q_{in,i}$  is the HBV output for both the current scenario and climate projections (Section 3.2).  $EF_m$  is estimated with the revised variable monthly flow method (RVFM) (Yu *et al.* 2021), combining the variable monthly flow method (VMF) (Pastor *et al.* 2014) with the Tennant method (Tennant 1976). RVFM assumes that  $EF_m$  is a percentage of the mean monthly flow (MMF) (Equation 7).

$$EF_m = \varphi \cdot MMF_m \quad (7)$$

where  $EF_m$  is the environmental flow in the  $m$ th month,  $MMF_m$  is the mean monthly flow in the  $m$ th month; and  $\varphi$  is the flow coefficient that varies from zero to one considering six ecological conditions in the river (poor, fair, good, excellent, outstanding, and optimum) and the month. A given month can be defined as a high-flow month if  $MMF_m$  is higher than 80% of the mean annual flow (*MAF*), and as a low-flow month if  $MMF_m$  is lower than 40% of *MAF*. Otherwise, it will be an intermediate-flow month (Table 3). The flow coefficients of Yu *et al.* (2021) (Table 3) can be used in temperate and subtropical climates, as regions with these conditions have similar

**Table 3.** Values of the flow coefficient ( $\phi$ ) associated with the ecological condition (poor, fair, good, excellent, outstanding, and optimum) and hydrological season (high-flow, intermediate-flow and low-flow months) in the revised variable monthly flow method. Extracted from Yu *et al.* (2021).

Months	Poor	Fair	Good	Excellent	Outstanding	Optimum
High-flow	0.10	0.30	0.40	0.50	0.60	0.70
Intermediate-flow	0.15	0.45	0.55	0.65	0.75	0.85
Low-flow	0.20	0.60	0.70	0.80	0.90	1.00

values of the  $\phi$  coefficient in the VMF method proposed by Pastor *et al.* (2014).

*MMF* and *MAF* have been obtained from the observed daily inflow discharge time series at the Eugui reservoir.  $EF_m$  does not change in the future, as it is assumed that  $EF_m$  is the minimum discharge required to sustain freshwater ecosystems downstream of the dam. Water supply demands and outflow discharge for energy production have been calculated and represent a percentage of  $EF_m$ . Moreover, the water released by the dam for the energy production and the water demands also supplies freshwater for the downstream ecosystem. Therefore, a further contribution in the outflow discharge is not included in Equation (4).

For each day,  $Q_{out,i}$  is quantified. A mass balance is applied with  $Q_{in,i}$  as input volume, the water volume that directly evaporates from the reservoir and  $Q_{out,i}$  as output volumes, obtaining the reservoir water level for the next day ( $WL_{i+1}$ ). In addition, storage water volumes at the reservoir in each day are also calculated.

The 36 parameters of the reservoir operation model ( $\alpha_m, \beta_m, \gamma_m$ ) are calibrated by comparing the observed and modelled mean daily reservoir water levels in the current scenario (2008–2021).  $Q_{in,i}$ , obtained with the calibrated HBV model, is used to calibrate the reservoir operation model, although observed daily inflow discharges are also available in the current scenario.

$Q_{in,i}$  simulated by the HBV model is the input data for the calibrated reservoir operation model and the results are time series of future daily reservoir water levels in the time window 2010–2100. A reservoir water level frequency curve is obtained for the three-time windows (2011–2040, 2041–2070, 2071–2100), in order to generate random initial reservoir water levels in the stochastic procedure (Section 3.4).

### 3.4 Stochastic procedure

A stochastic procedure is used to generate a large set of inflow hydrographs with random inflow peaks ( $Q_{peak}$ ) and initial reservoir water levels ( $WL_{ini}$ ). Two random probability vectors are generated independently, as no clear correlation has been detected in the pairs of  $Q_{peak}$  and  $WL_{ini}$  in the observations. Ten thousand values of  $Q_{peak}$  and  $WL_{ini}$  are generated for each of the 72 scenarios considered in the study, given by the combination of 12 climate models, three future time windows and two RCPs. The random vector of  $Q_{peak}$  represents the non-exceedance probabilities (*NEPs*) of peak inflow hydrographs. The random vector of  $WL_{ini}$  characterizes the exceedance probability (*EP*) of reservoir water levels. The two vectors are randomly combined to obtain the feasible combinations of the  $Q_{peak}$ – $WL_{ini}$  pairs (Fig. 4).

While a low *EP* of  $WL_{ini}$  is associated with a high initial reservoir water level (red lines in Fig. 4(c)), a value close to one represents low reservoir water levels (dark blue line in Fig. 4(c)). A high *NEP* of  $Q_{peak}$  corresponds to a high inflow peak associated with a high return period (*RP*) (red line in Fig. 4(b)).

The relationship between *NEP* (or *RP*) and  $Q_{peak}$  is characterized with a GEV distribution function fitted to the RIBS model outputs obtained in Lompi *et al.* (2021). The hydrograph shapes supplied by the RIBS model outputs are associated with each value of  $Q_{peak}$ . Each *EP* value for  $WL_{ini}$  is associated with a given reservoir water level using the empirical reservoir water level frequency curve obtained by coupling the HBV and reservoir operation models (Sections 3.2 and 3.3).

### 3.5 Volumetric evaluation method

VEM is a flood-routing reservoir model that can simulate outflow discharges from gated dam spillways during a flood event (Girón 1988). The main differences between VEM and the reservoir operation model (Section 3.4) regard the time step and the operation of spillway gates in flood events. The reservoir operation model uses a daily scale, useful to simulate daily reservoir water levels, although its time resolution is too coarse to properly simulate flood control processes at sub-daily time scales. However, VEM uses sub-hourly time steps, considering spillway gate operations, reservoir water level and outflow discharge variations at a higher temporal resolution. In this study, inflow hydrographs with a 15-min time step are used.

VEM assumes that, considering constant inflow  $Q_{in,t}$  and outflow discharges  $Q_{out,t}$  when  $Q_{in,t}$  is greater than  $Q_{out,t}$ , the number of remaining time steps ( $N_t$ ) before the maximum reservoir storage capacity ( $V_{max}$ ) will be reached is:

$$N_t = \frac{V_{max} - V_t}{(Q_{in,t} - Q_{out,t}) \cdot \Delta t} \quad (8)$$

where  $V_t$  is the reservoir storage volume at time  $t$ ;  $Q_{in,t}$  is the inflow discharge at time  $t$ ;  $Q_{out,t}$  is the outflow discharge at time  $t$ ; and  $\Delta t$  is the inflow hydrograph time step. When the reservoir is filled, inflow and outflow discharges must be the same to avoid overtopping. Therefore, VEM is based on a linear increasing of  $Q_{out,t}$  values, to reach  $Q_{in,t}$  in the  $N_t$  time steps. Therefore,  $Q_{out,i}$  must increase  $\Delta Q_{out,t}$  in each time step (Equation 9).

$$\Delta Q_{out,t} = \frac{Q_{in,t-1} - Q_{out,t}}{N_t} = \frac{(Q_{in,t-1} - Q_{out,t})^2}{V_{max} - V_t} \Delta t \quad (9)$$



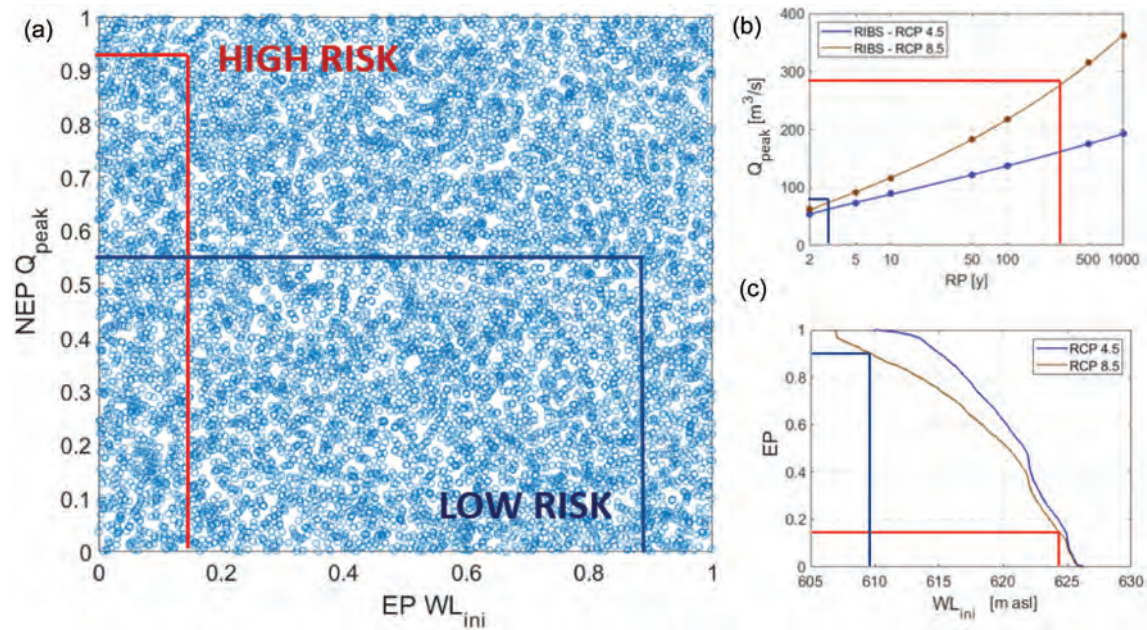


**Figure 4.** Random generation of peak discharge and initial water levels ( $Q_{peak}$ - $WL_{ini}$  pairs). (a) Feasible space of  $Q_{peak}$ - $WL_{ini}$  pairs; (b) non-exceedance probabilities (NEPs) associated with  $Q_{peak}$  represented with return periods (RPs); (c) exceedance probabilities (EP) of  $WL_{ini}$ .

Outflow discharge released by the spillway ( $Q_{out,t}$ ) is obtained in each time step with Equation (9), producing outflow hydrographs. VEM uses the 10 000 inflow hydrographs associated with the 10 000 random initial reservoir water volumes in each scenario to obtain the 10 000 maximum reservoir water levels ( $WL_{max}$ ). RP quantiles of  $WL_{max}$  are estimated from the empirical frequency curve of  $WL_{max}$  for each scenario.

### 3.6 Uncertainty assessment

Uncertainty assessment in the simulation chain aims to consider all sources of error in the methodology. Several tools and methodologies are available to account for uncertainty (Refsgaard *et al.* 2007, Matott *et al.* 2009), as well as guidance to identify the most suitable uncertainty assessment tool (Van Der Keur *et al.* 2010). Katz (2002) recommends to *disintegrate* the uncertainty analysis and assess each element separately within an integrated framework. According to Morales-

Torres *et al.* (2016), climate-related uncertainties have the greatest impact on risk analysis models for dam management. Indeed, high return periods are usually involved in dam risk analysis, but the time series length of observed data is not adequate for their characterization. For this reason, several studies have proposed to incorporate climate uncertainty in dam management both in future (Fluixá-Sanmartín *et al.* 2021) and in the current scenario (Tarouilly *et al.* 2021).

The main sources of uncertainty in this study arise from both inflow hydrograph and reservoir water level probability estimates. Inflow hydrograph estimates in the future, i.e. future flood quantiles, have two sources of uncertainty: (i) uncertainty in delta changes of precipitation associated with a given return period (red in Fig. 5), and (ii) errors in design peak discharge estimates obtained with the RIBS model (blue in Fig. 5). In addition, the main source of uncertainty in initial reservoir water level estimates comes from errors in HBV model simulations (green in Fig. 5).

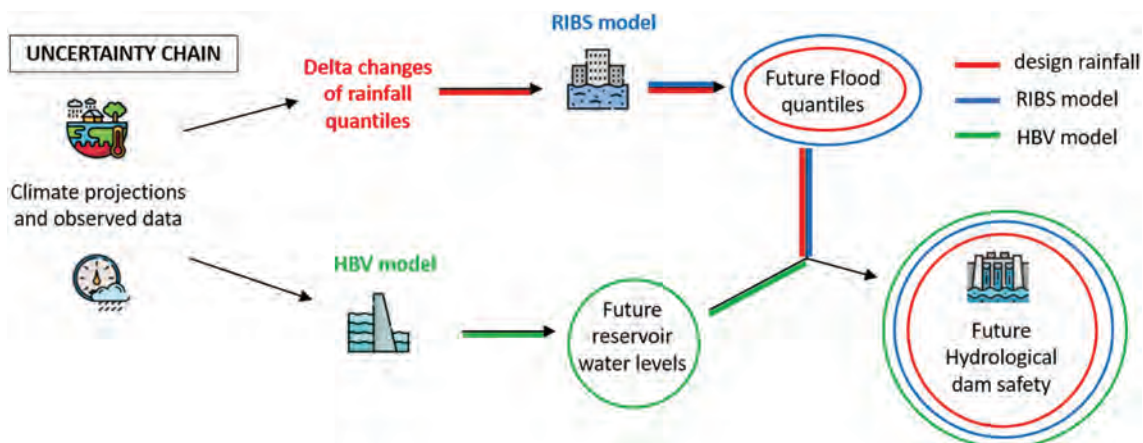


**Figure 5.** Uncertainty chain in the evaluation of hydrological dam safety. Three sources of errors are assessed: design rainfall uncertainty is red, and the uncertainty of the hydrological models is blue for RIBS and green for HBV. (Icons made by Sittipat Tojarean, Good Ware, Freepik and Umeicon from [www.flaticon.com](http://www.flaticon.com)).

First, the uncertainty in delta changes of precipitation quantiles obtained by Garijo and Mediero (2019) is assessed, as precipitation quantile estimates are obtained using short rainfall time series. Uncertainty is quantified by generating a set of 10 000 time series of annual maxima with a length of  $N_{obs}$  years, where  $N_{obs}$  is the number of years considered in each time window of the current and future periods to estimate rainfall quantiles. Delta changes of rainfall quantiles are obtained by comparing precipitation quantiles in a given time window with the control period. Therefore, 10 000 values of delta changes are obtained for each return period and scenario (combination of climate model, RCP, and time window). Ten thousand mean values of precipitation in the Eugui Dam catchment are calculated for each return period and scenario by analysing together the spatial distribution of delta changes and the spatial distribution of the raingauges used to determine the design rainfall in the current scenario, replicating the methodology of Lompi *et al.* (2021).

A support vector machine is trained to reproduce the performance of the RIBS model using the simulations run in Lompi *et al.* (2021) to avoid the long computation times that would require the fully distributed hydrological model to simulate 5 040 000 events. Therefore, 10 000 values of peak flows are obtained for each return period and scenario, considering the precipitation values generated above.

The RIBS model uncertainty in the estimation of peak discharges is considered with a parameter  $K_{RIBS}$  that represents the ratio between the observed,  $Q_{peak,obs}$ , and the modelled,  $Q_{peak,RIBS}$ , peak discharges. The observed peaks refer to the real event considered in the calibration of the model.

$$K_{RIBS} = \frac{Q_{peak,obs}}{Q_{peak,RIBS}} \quad (10)$$

A normal probability distribution is fitted to the  $K_{RIBS}$  values, to generate random  $K_{RIBS}$  values for each peak flow, aiming to consider the uncertainty of the RIBS model.

Seven percentiles are extracted from each set of 10 000 peak discharge values for each return period: 5%, 10%, 32%, 50%, 68%, 90%, and 95%. A GEV distribution is fitted to the peak flow quantiles obtained for each percentile (Fig. 6). For each GEV distribution, 10 000 random NEPs (or RPs) values are generated (Section 3.4). Hydrograph shapes supplied by the RIBS model are associated with each  $Q_{peak}$  value.

Uncertainty in HBV model outputs is considered by calculating the  $K_{HBV}$  coefficient, which is the ratio between the daily observed and modelled discharges obtained after the calibration of HBV, similarly to Equation (10) for the RIBS model. A normal distribution is fitted to the  $K_{HBV}$  values. A random  $K_{HBV}$  value is generated each day with such a normal distribution to include uncertainty in  $Q_{in,i}$  that is the input data in the reservoir operation model (Equation 6). The uncertainty in HBV model outputs is considered to assess the uncertainty in the initial water level frequency curve. The complete time series of inflow discharge is corrected 50 times with random daily  $K_{HBV}$  values, as producing 10 000 simulations with the reservoir operation model for each scenario is unaffordable due to the computational cost. A sensitivity analysis concluded that 50 simulations were sufficient, as the difference between the mean water level frequency curve obtained with 50 and 10 000 simulations was negligible. The reservoir water level frequency curve considered for estimating initial reservoir water levels is obtained as the mean value of the 50 water reservoir level frequency curves. A given initial reservoir water level is assigned to each synthetic inflow hydrograph.

### 3.7 Overtopping probability and delta changes estimates

The impact of climate change on hydrological dam safety is assessed using the overtopping probability and delta changes in maximum reservoir water level. Delta changes of maximum reservoir water levels ( $\Delta WL$ ) are obtained with Equation (11).

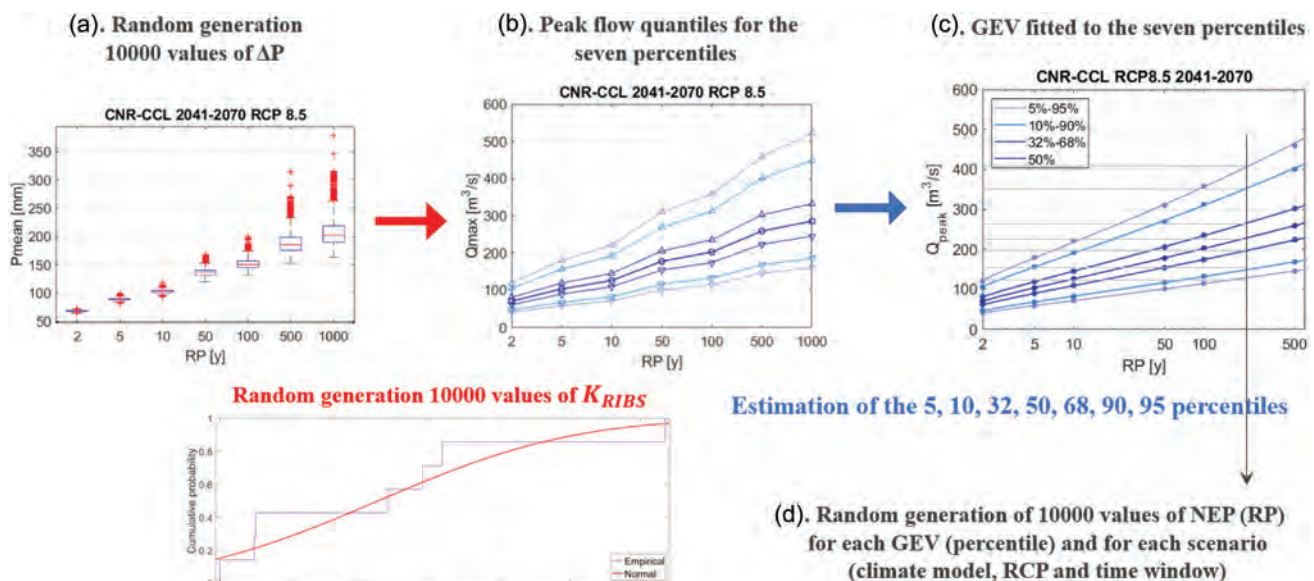


Figure 6. Stochastic procedure to incorporate the uncertainty in inflow hydrograph estimates.

$$\Delta WL(RP_i, 50^{th}) = WL_{fut}(RP_i, 50^{th}) - WL_{cur}(RP_i, 50^{th}) \quad (11)$$

where  $WL_{fut}(RP_i, 50^{th})$  is the maximum reservoir water level expected in the future associated with a given return period  $RP_i$  for the 50<sup>th</sup> percentile after the uncertainty incorporation, and  $WL_{cur}(RP_i)$  is the maximum reservoir water level in the current scenario for the return period  $RP_i$  and the 50<sup>th</sup> percentile. If  $\Delta WL$  is greater than zero, the maximum reservoir water level expected in the future will be greater than the current scenario. If  $\Delta WL$  is lower than zero, the maximum reservoir water level expected in the future will decrease.  $\Delta WL$  is obtained as the difference between the future and control periods, as all delta changes would be close to one if the ratio between water levels above sea level is considered.

The overtopping probability is the EP of the reservoir water level that corresponds to the maximum reservoir storage capacity at the dam crest. In addition, potential wave heights generated by wind are also considered with the Stevenson formula (Stevenson *et al.* 1981) (Equation 12) that can be used when no wind data are available. Therefore, overtopping is assumed to occur when the reservoir water level equals the dam crest elevation minus the wave height.

$$h_w = 0.76 + 0.34 \cdot \sqrt{F} - 0.26\sqrt[4]{F} \quad (12)$$

where  $h_w$  is the wave height (m); and  $F$  is the fetch (km), which is the longest path over water from the dam to any point in the reservoir. The height considered in the study is four thirds of  $h_w$ , as two thirds of  $h_w$  is above the reservoir water level for a given wave, and water jumps to two thirds of  $h_w$  above the wave crest when it hits the dam upstream face.

## 4 Results

This section presents the results of the methodology applied to the Eugui Dam case study. The results of the statistical analysis with observed data are shown in Section 4.1; the reservoir water levels and peak inflow

discharges obtained in the future are presented in Section 4.2; and the findings on the changes in maximum reservoir water levels are in Section 4.3. Finally, the results that include the uncertainty assessment are given in Section 4.4.

### 4.1 Statistical analysis of observed data

A GEV distribution function is fitted to the AMS of 42 years of peak inflow discharges in the period 1979–2020 (Fig. 7(a)). In addition, the empirical distribution of reservoir water levels in the current scenario is obtained with 15-min observations in the period 1998–2021 (Fig. 7(b)). The two frequency curves are used in the stochastic procedure to assess the maximum reservoir water level frequency curve in flood events in the current scenario.

The maximum inflow peak discharge observed at the reservoir is 131.3 m<sup>3</sup>/s. The inflow peaks associated with return periods of 100, 500 and 1000 years are 170.9, 245.8 and 285.1 m<sup>3</sup>/s, respectively.

The reservoir water levels oscillate between 615 and 626 m a.s.l. However, a reservoir water level of 620 m a.s.l. has an exceedance probability of around 90%. In addition, the EP of the water level at the spillway crest elevation (625 m a.s.l.) is 29%. The maximum reservoir water level recorded is 627.5 m a.s.l. Therefore, the EP of the water level associated with the upper limb of the gates (628 m a.s.l.) is zero in the period with observations.

### 4.2 Reservoir water levels and peak inflows in the future

The HBV model is calibrated in the Eugui Dam catchment with 13 years of observations (2008–2021). Figure 8 shows the results just in the period 2019–2022. A set of 20 000 random combinations of the 11 HBV model parameters is considered using Monte Carlo simulations. The efficiency of the model, quantified by the  $R_{eff}$  statistic, is 0.8556; this reaches the calibration target, as the  $R_{eff}$  value is greater than 0.85. The performance of the model in the validation period remains

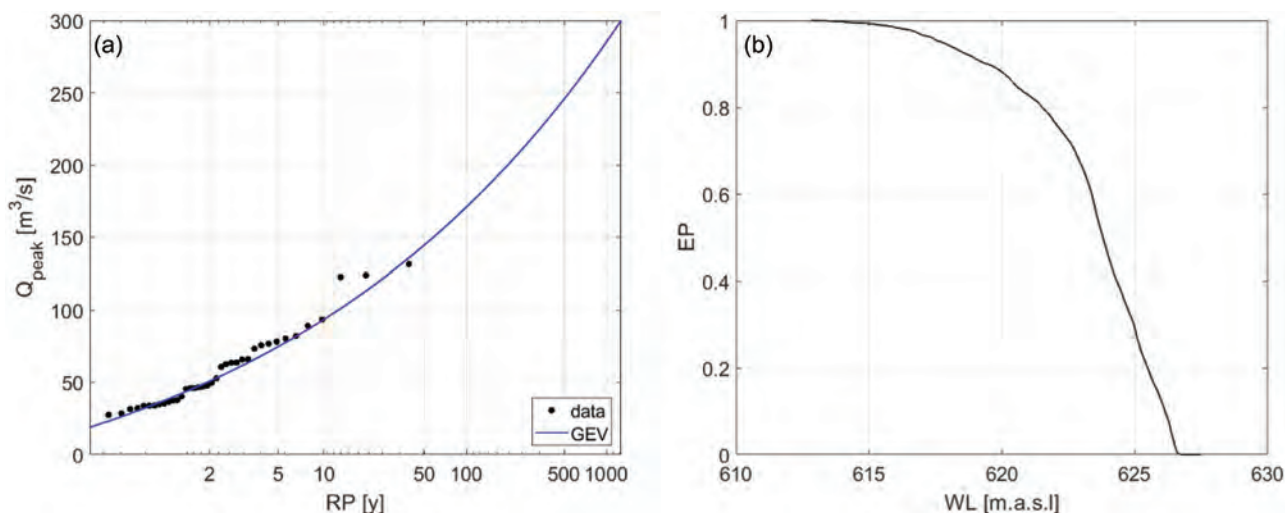
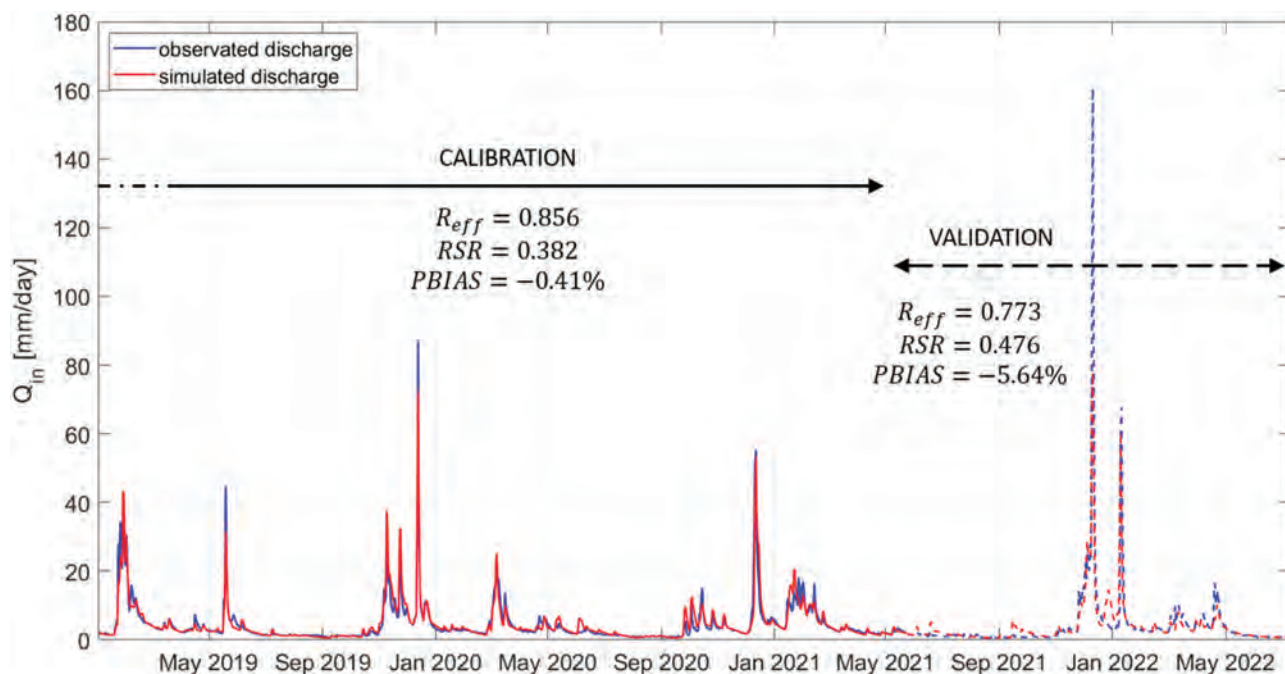


Figure 7. Frequency curves in the current scenario: (a) peak inflow discharges in the reservoir; (b) reservoir water levels.



**Figure 8.** Results of the calibration (solid line) and of the validation (dashed line) of the HBV model in the period 2019–2022. The blue line represents the observed daily discharges by the HBV model, while the red line shows the observations.

good according to Moriasi *et al.* (2015):  $R_{eff}$  ( $NSE$ ) is equal to 0.773,  $RSR$  is 0.476 and  $PBIAS$  is  $-5.64\%$ .

Monthly environmental flows ( $EF_m$ ) used in the reservoir operation model are presented in Table 4. The time series of daily inflow discharges to the Eugui reservoir simulated by the HBV model in the current scenario (2008–2021) are used as input data for the reservoir operation model described in Section 3.3, to simulate daily reservoir water levels in the last 13 years. The reservoir operation model is also calibrated using Monte Carlo simulations, aiming to reduce the bias between daily simulated and observed reservoir water levels. Varying values of the 36 parameters  $\alpha_m$ ,  $\beta_m$ ,  $\gamma_m$  of the reservoir

operation model have been considered (Section 3.3), analysing the  $RMSE$  and  $NSE$  between observed and simulated daily water levels. Figure 9 shows that the simulated frequency curve of  $WL$  is close to the frequency curve fitted to observations.

Moreover, the Kolmogorov-Smirnov two-sample statistical test is conducted on the two empirical cumulative distributions, and the  $p$  value of .044 shows that the calibration of the reservoir operation model is good. Indeed, the closer the  $p$  value is to 0, the more likely it is that the two samples come from the same distribution. Nevertheless, this is just intended to assess the goodness of the calibration as the

**Table 4.** Monthly environmental flows used in the reservoir operation model.

Month	Jan	Feb	Mar	Apr	May	Jun	Jul	Aug	Sep	Oct	Nov	Dec
$EF_m$ [ $m^3/s$ ]	2.51	2.72	2.46	1.87	1.43	1.44	1.02	0.92	0.93	1.20	1.87	2.18

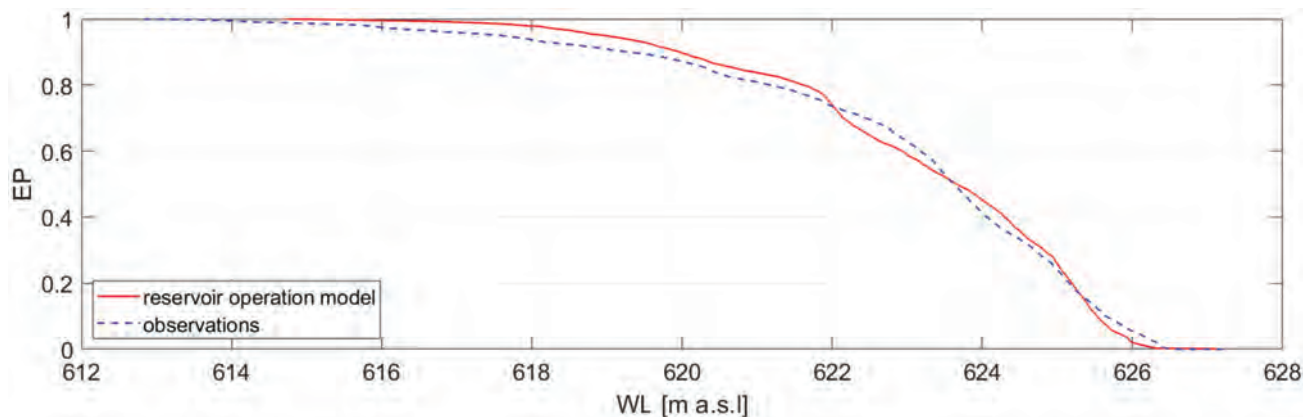


**Figure 9.** Calibration results for the reservoir operation model. The dashed blue line represents the empirical frequency curve of reservoir water levels extrapolated from the observations. The red line represents the reservoir water levels simulated by the reservoir operation model.

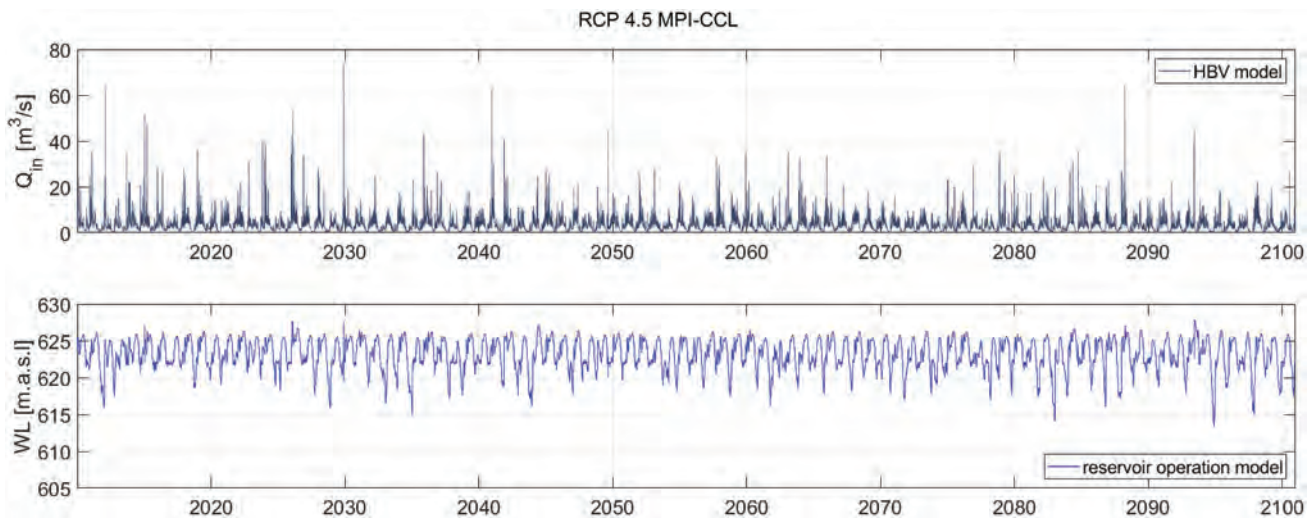


**Figure 10.** Results for the MPI-CCL climate model and RCP 4.5 in the period 2006–2100. (a) Inflow discharge time series in the reservoir simulated by the HBV model; (b) reservoir water levels obtained by the reservoir operation model.

empirical frequency curves do not come from a given distribution, as they are the results of a hydrological model rather than a statistical analysis.

Future initial reservoir water levels for each climate model, RCP and future period are assessed. Climate projections of rainfall and temperature are used as input data for the calibrated HBV model, obtaining time series of daily inflow discharges in the reservoir ( $Q_{in}$ ) (Fig. 10(a)). The calibrated reservoir operation model uses  $Q_{in}$  as input data to simulate the time series of daily reservoir water levels (Fig. 10(b)).

Three future periods are considered – 2011–2040, 2041–2070, and 2071–2100 – corresponding to the periods used in

Lompi *et al.* (2021). Initial reservoir water level frequency curves are obtained from the outputs of HBV and reservoir operation models (Fig. 11). Figure 11 shows the impact of climate change on initial reservoir water levels expected at the beginning of flood events. In the future, reservoir water levels are expected to decrease compared with water levels in the current scenario. Such a decrease is clear for the 12 climate models in both RCPs, but it is greater in RCP 8.5 than in RCP 4.5. In addition, flood peaks will increase over time for RCP 8.5, with the greatest changes expected in the 2071–2100 time window. Therefore, the greatest flood events will encounter lower reservoir initial water levels.

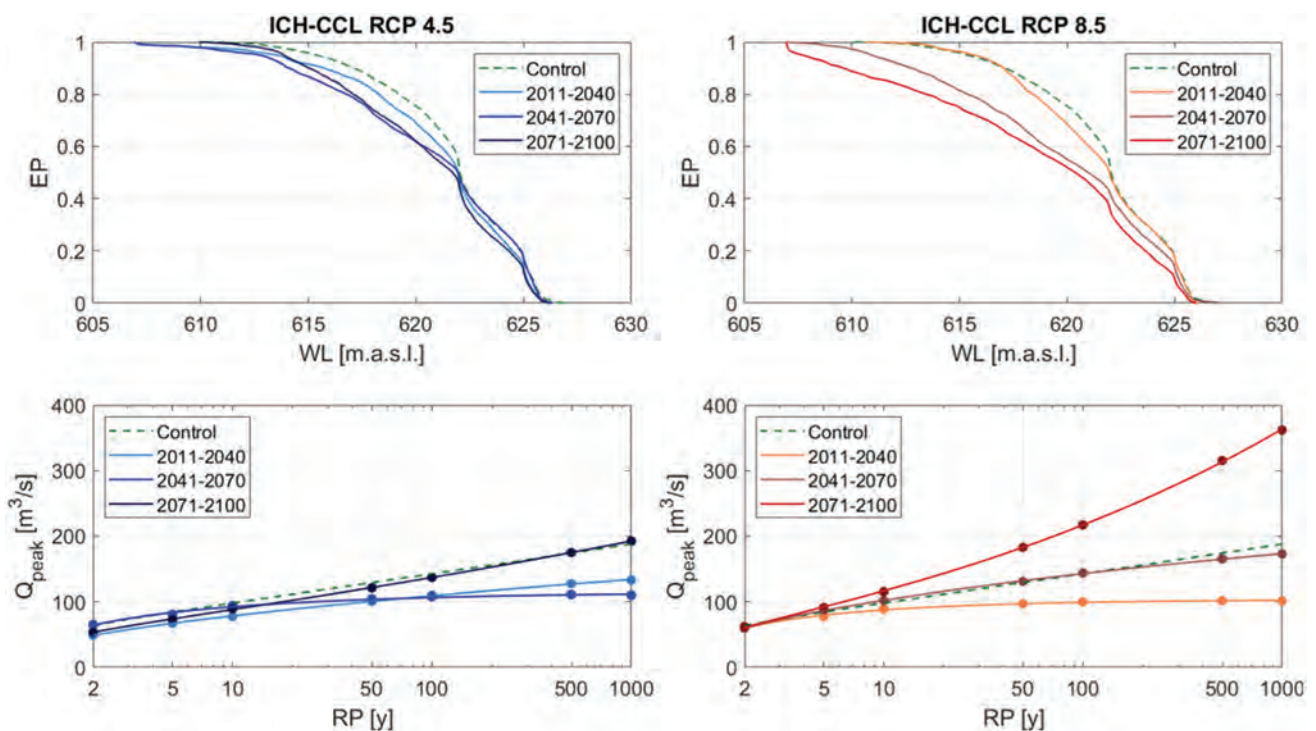


**Figure 11.** Initial reservoir water level and inflow peak discharge frequency curves for the ICH-CCL climate model in the three time windows. The left column shows the results for RCP 4.5. The right column offers the results for RCP 8.5. Each time window is represented with a different colour. Control periods are illustrated with dashed lines and future periods with solid lines.

### 4.3 Changes in maximum reservoir water levels

Figure 12 shows the expected elevations of maximum reservoir water levels ( $WL_{max}$ ) in flood events for the IPS-WRF climate model. The dam is represented in grey, showing that the maximum water levels should not exceed the dam crest elevation at 630 m a.s.l. In addition, the overtopping threshold is fixed to the elevation of 628.71 m a.s.l., to consider potential wave heights induced by wind (Section 3.7). If  $WL_{max}$  exceeds the overtopping threshold, it is assumed that water can exceed the dam crest. Figure 12 also shows the expected delta changes in maximum reservoir water levels ( $\Delta WL$ ).  $\Delta WL$  positive values point to an increase in the maximum reservoir water levels in flood events in the future.  $\Delta WL$  negative values indicate a decrease in the maximum reservoir water levels in flood events in the future.

Figure 12 shows how the operation of spillway gates can maintain the maximum reservoir water level at the elevation of their upper limb (628 m a.s.l.) for the events with an  $RP$  between five and 500 years, despite the fact that inflow peak discharges associated with different return periods can differ. Nevertheless, maximum peak outflow discharges increase for the highest return periods to avoid exceeding the elevation of the upper limb of the spillway gates. Only a slight increase in the maximum reservoir water level for the 500- and 1000-year  $RP$  is obtained for RCP 4.5 in the 2011–2040 time window. Similarly, the greatest expected changes in maximum reservoir water levels in RCP 4.5 for the 1000-year flood are found in the 2011–2040 time window for 10 out of 12 climate models. Figure 12 also shows how the greatest expected changes of maximum water levels are in the 2041–2070 time window for

RCP 8.5, where the maximum reservoir water level can cause dam overtopping. Nevertheless, the IPS-WRF climate model is the only one with these highest water levels expected in such a time window. Indeed, while five of the 12 climate models show that the greatest maximum water levels are expected at the end of the century in RCP 8.5, in six climate models no changes are expected in this emission scenario.

### 4.4 Uncertainty assessment

GEV distribution functions are fitted to the 12 climate models (Fig. 6) for the three time windows (2011–2040, 2041–2070), two emission scenarios (RCP 4.5, RCP 8.5) and seven percentiles (5%, 10%, 32%, 50%, 68%, 90% and 95%) to consider the uncertainty in inflow peak estimates. Figure 13 shows the results considering the uncertainty chain, representing the maximum reservoir water level frequency curve for the seven percentiles. Moreover, the results obtained previously without accounting for the uncertainty shown in Fig. 12 are also presented, with red dots.

Figure 13 highlights the importance of considering uncertainty in the methodology. In some cases, the uncertainty assessment supplies a confidence interval to the results obtained without uncertainty, and the red dots overlap the curve for the 50<sup>th</sup> percentile, as for example in the 2041–2070 time window for RCP 8.5. In other cases, the results without considering the uncertainty (red dots) are below the median values obtained considering uncertainty, usually underestimating the maximum reservoir water levels. For example, for the time window 2071–2100 in RCP 8.5, the results obtained

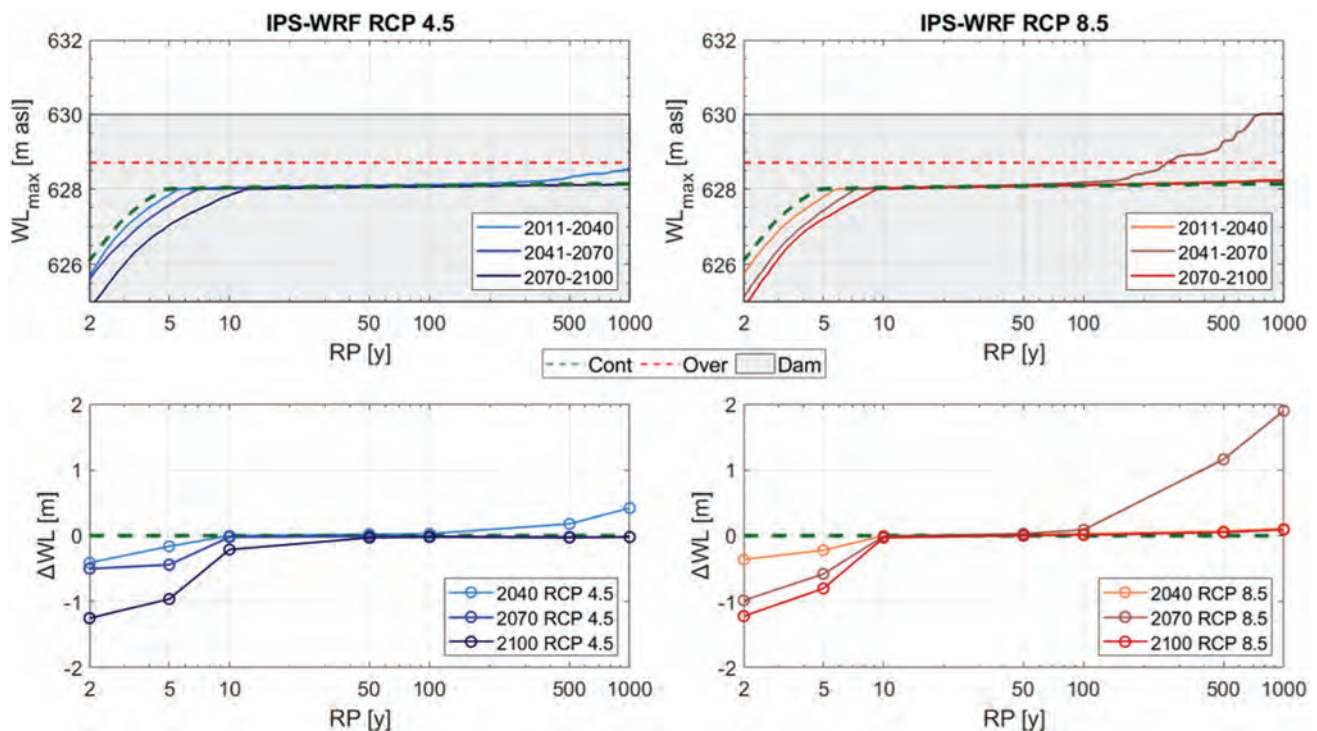


**Figure 12.** Comparison of maximum reservoir water level frequency curves in the three periods in the future with the control period for the IPS-WRF climate model. The top row shows maximum reservoir water level elevations and the bottom row shows the delta changes in maximum reservoir water levels. The horizontal dashed red line that crosses 628.7 m a.s.l. in the upper figures represents the overtopping threshold. The grey box represents the dam with its crest elevation at 630 m a.s.l. The dashed green line in all the sub-plots represents the control period. Future periods are represented with solid lines for RCP 4.5 on the left and for RCP 8.5 on the right.

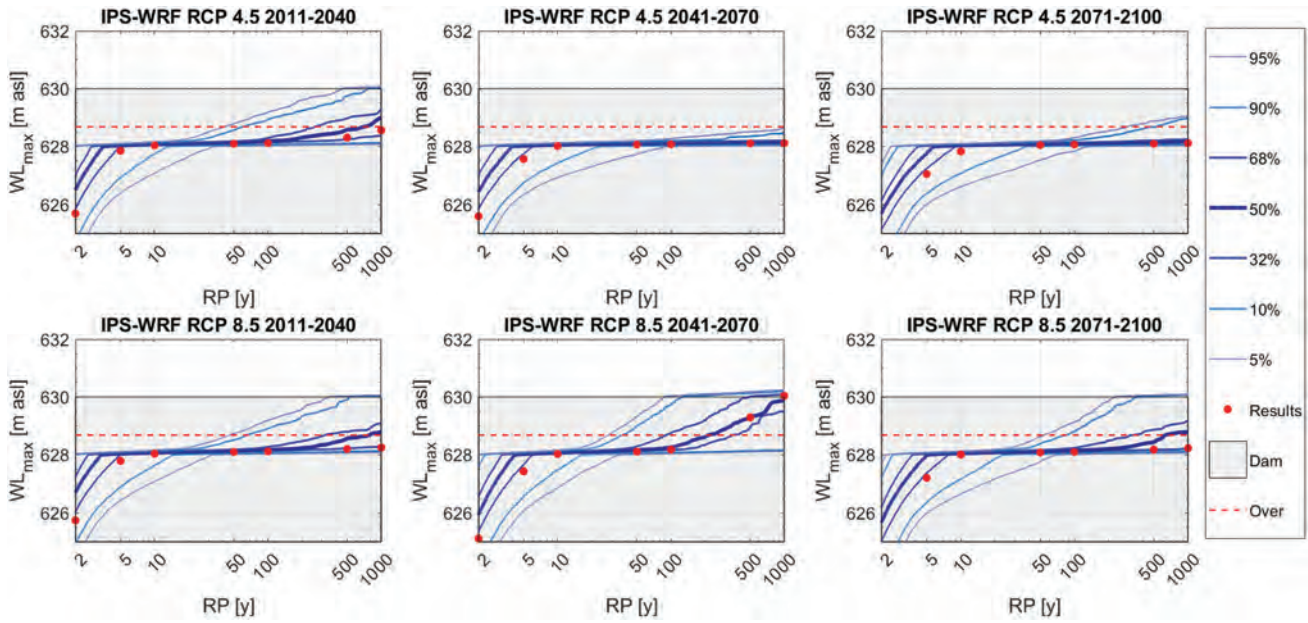


**Figure 13.** Expected maximum reservoir water levels in the future for the IPS-WRF climate model considering uncertainty. The top row includes the results for RCP 4.5 and the bottom row includes the results for RCP 8.5. Columns present results by time windows in the future. The thickest solid blue line represents the median values. Thinner solid light blue lines represent the rest of the percentiles. Red points represent the results without considering uncertainty for the seven return periods. The grey box represents the dam with its crest elevation at 630 m a.s.l. The horizontal dashed red line represents the overtopping threshold.

without assessing the uncertainty do not point to an increase in the hydrological dam risk, although an increase of almost 1 m is expected when the uncertainty is considered.

A complete overview can be obtained by joining the results of the 12 climate models. For a given scenario, delta changes in maximum reservoir water levels are quantified with the difference between their median value (50<sup>th</sup> percentile) and the control period (Section 3.7). Delta changes for the 12 climate models are joined in the box plot shown in Fig. 14. The expected maximum reservoir water levels in the

future can be obtained by applying the delta changes to the maximum reservoir water level frequency curve in the current scenario (Fig. 14), offering information about the expected changes in maximum reservoir water levels. The information about the overtopping probability is shown in Table 5 and Fig. 15, where the probabilities for the 12 climate models, scenarios and time windows are extracted from the 50<sup>th</sup> percentiles after the uncertainty incorporation. Figure 14 (a) shows that no overtopping risk is expected for events with an *RP* below 1000 years in the current scenario. The

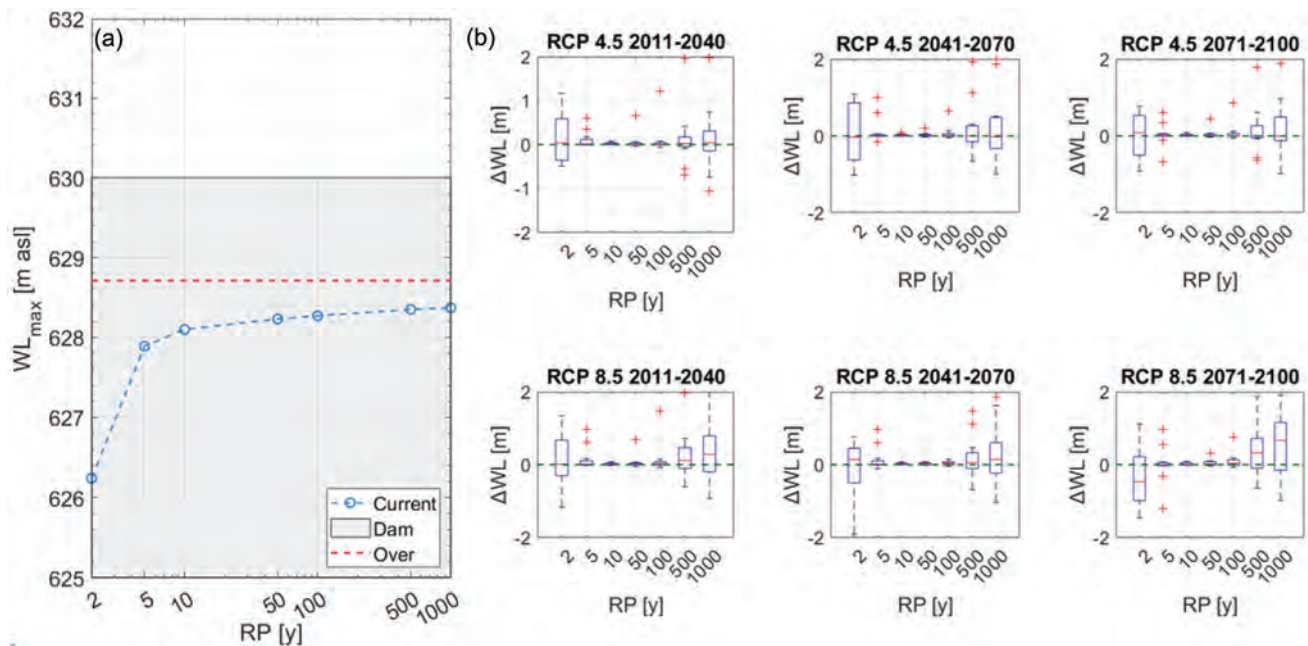


**Figure 14.** (a) Maximum reservoir water level frequency curve in the current scenario; (b) delta changes in maximum reservoir water levels for the ensemble of 12 climate models considering uncertainty.

**Table 5.** Extracted overtopping probability obtained with the 50<sup>th</sup> percentile for the 12 climate models considering the incorporation of uncertainty. Zero values correspond to probabilities smaller than  $10^{-4}$ .

Climate model	RCP 4.5			RCP 8.5		
	2011–2040	2041–2070	2071–2100	2011–2040	2041–2070	2071–2100
ICH-CCL	0	0	0	0	0	0.0023
MPI-CCL	0.0208	0.0105	0.0157	0.0214	0.0016	0.0121
MOH-RAC	0	0	0	0	0	0
CNR-CCL	0	0.0037	0.0021	0.0018	0.0006	0.0026
ICH-RAC	0	0.0009	0.0016	0.0001	0	0.0005
MOH-CCL	0	0	0.0002	0.0033	0	0.0028
IPS-WRF	0.0012	0	0	0.0012	0.0042	0.0014
IPS-RCA	0.0007	0.0003	0	0.0011	0.004	0.0004
MOH-RCA	0	0	0	0	0	0
ICH-RCA	0	0.0003	0.0001	0.0003	0.0004	0.0023
CNR-RCA	0.0009	0	0.0007	0	0.0002	0
MPI-RCA	0.0002	0	0	0.0006	0.0006	0.0018

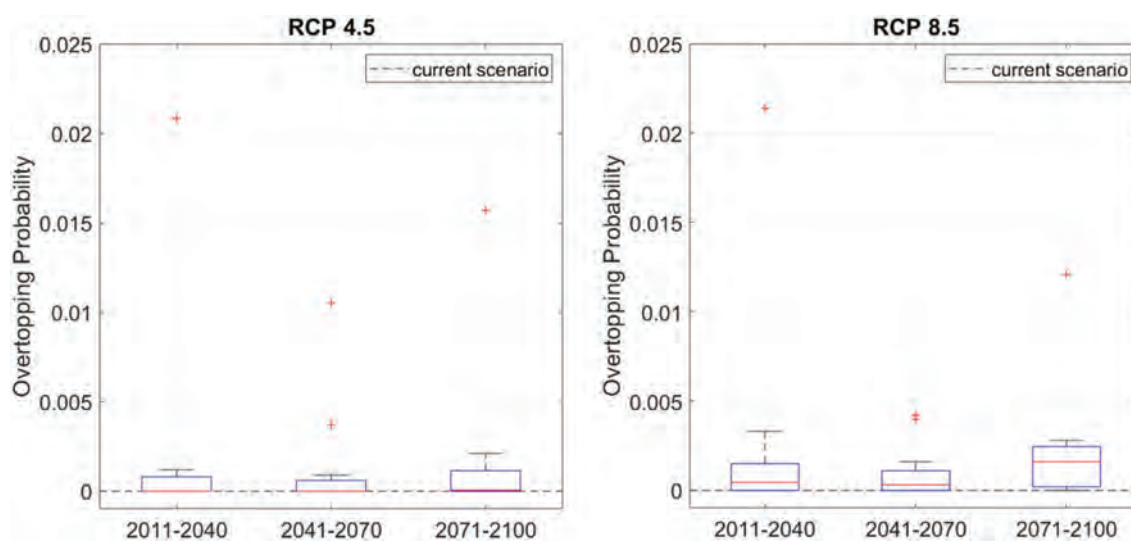


**Figure 15.** Overtopping probability with the ensemble of the 12 climate models accounting for the uncertainty in the three time windows. (a) RCP 4.5; (b) RCP 8.5. The dashed black line represents the overtopping probability in the current scenario, which is zero as it is lower than  $10^{-4}$ .

delta changes for the 50<sup>th</sup> percentile, for RPs between 5 and 500 years in the three time windows and two emission scenarios, point to no expected changes in maximum reservoir water levels in the future with high confidence. This is because the spillway gate operation can maintain the maximum water level at 628 m a.s.l. for the magnitude of such events. Nevertheless, despite dam operations that can maintain the maximum water level at 628 m a.s.l., outflow discharges will increase to maintain such a level in those RPs. A higher variability is found in the results associated with the RP of 2, 500 and 1000 years. In the first case, the variability is generated by many cases in which maximum reservoir water levels are below 628 m a.s.l., which is the water level when the spillway gates begin to operate. For extreme events with return periods of 500 and 1000 years, the variability is driven by water levels above 628 m a.s.l., as dam operations are not able to maintain such a water level because the spillway does not have sufficient capacity to release the outflow discharges required to avoid increasing water levels.

Table 5 shows the number of climate models with an overtopping probability greater than  $10^{-4}$  in each scenario. Zero values correspond to probabilities smaller than  $10^{-4}$ , as each scenario is characterized by 10 000 synthetic events. The

current scenario has an overtopping probability equal to zero as the most extreme synthetic event causes a reservoir maximum water level of 628.45 m a.s.l., which is under the overtopping threshold (628.71 m a.s.l.). Dam overtopping is more likely to occur in RCP 8.5 in the 2071–2100 time window, where nine climate models show a probability greater than zero. This is evident by analysing the median values of the box plots that ensemble the dam overtopping probabilities in Fig. 15. Only RCP 8.5 has non-zero median values, especially in the time window 2071–2100 when the dam overtopping probability is 0.0016 (RP = 625 years).

## 5 Discussion

The decreasing pattern in initial water levels at the beginning of flood events in Fig. 11 agrees with the results of many other studies. Indeed, a warmer climate will lead to a decrease in reservoir storage volumes because catchment runoff volumes will decrease and evapotranspiration rates will increase at the Eugui Dam, as detected by Konapala *et al.* (2020) globally. These results also agree with Fluixá-Sanmartín *et al.* (2019b), who found similar results in another dam in western Spain. In this study, such decreasing reservoir water levels are related to



two different drivers. First, a greater mean temperature in the Eugui Dam catchment will increase evapotranspiration rates in the reservoir, decreasing water storage volumes, and reducing soil moisture content in the catchment. Second, a lower mean annual precipitation in the catchment will reduce runoff volumes, decreasing reservoir water storage volumes and levels. In addition, the decreasing trend in reservoir storage volumes in the future at the Eugui Dam agrees with the reduction of water availability in some Mediterranean lakes (Bukac *et al.* 2017) and catchments (Iglesias *et al.* 2007). Moreover, global annual mean reservoir evaporation rates are expected to increase by 16% by 2100 (Woolway *et al.* 2020). Furthermore, mean annual streamflows are projected to decrease in the southern part of Europe (Blöschl *et al.* 2019).

Lompi *et al.* (2021) found the greatest expected changes in flood quantiles in the 2011–2040 time window in RCP 4.5, when the peak of emission occurs. In this study, 10 of the 12 climate models also show the greatest delta changes of maximum water levels in such a scenario, pointing to a relationship between the future hydraulic dam safety and the greenhouse gas emission peak. However, this signal becomes negligible (median  $\Delta WL = 5$  cm) when the uncertainty is incorporated into the methodology and the ensemble of all climate models is considered (Fig. 14). Indeed, no increase in the overtopping probability is found in this scenario (Fig. 15). Figure 12 shows that the greatest changes of maximum water levels are expected in the 2041–2070 time window. This result may be just an anomaly, however, representing an outlier both in the ensemble of delta changes of maximum water levels (right part of Fig. 14) and in the overtopping probabilities (right part of Fig. 15). Moreover, the greatest expected changes in maximum reservoir water levels (right part of Fig. 14) are expected in the peak of emissions, i.e. the end of the 21<sup>st</sup> century in RCP 8.5, when the ensemble of all the climate models and uncertainty are considered. Indeed, even if the variability of the delta changes associated with the most extreme event is evident for both the emission scenarios, the median values of the box plots show an increase in the maximum reservoir water level only in RCP 8.5, especially in the 2071–2100 time window, with an increase of 0.67 m for the 1000-year flood. In addition, such an increase can generate dam overtopping when it is summed to the maximum reservoir water level in the current scenario. In other case studies, similar results were obtained by Mallakpour *et al.* (2019), who found that hydrological failure probability is likely to increase for most dams in California by 2100 in RCP 8.5, while the results do not agree with Fluixa-Sanmartin *et al.* (2019b), who found no clear signal for such a scenario, as in this case the higher probability of social and economic risk was found in RCP 4.5.

Uncertainty assessment has a key role in the evaluation of hydrological dam safety. Assessments carried out without incorporating uncertainty tend to underestimate both the delta changes of maximum water levels and the overtopping probabilities in all the climate models and scenarios. This could be driven by underestimates in rainfall quantiles and by the uncertainty in the RIBS hydrological model that tends to underestimate flood peaks at the Eugui Dam. Therefore, the inclusion of uncertainty with the coefficient  $K_{RIBS}$  tends to increase the results obtained without considering the uncertainty.

Future changes in land cover upstream of the dam can affect the overtopping risk, but in both the hydrological models this is not considered also because it is very uncertain. Climate change impacts not only hydrograph peak discharges but also flood volumes, with expected changes not necessarily proportional to the peak (Brunner *et al.* 2018). For this reason, an improvement of the proposed methodology could be the generation of random hydrograph shapes for the inflow hydrograph in the reservoir to also consider future flood volumes in a multivariate framework. Moreover, the stochastic procedure proposed in this study considers the impact of climate change on hydrological dam safety on an annual basis, not considering the seasonality of inflow peaks and reservoir water level frequency. However, peak discharge and initial reservoir water levels at the beginning of the flood event can depend on the season. Indeed, reservoir water levels are usually higher in late spring than in early autumn at the end of the dry season, as part of the storage volume is used for water supplies in summer. Therefore, future research will focus on the seasonality of the climate change impact on hydrological dam safety.

The proposed methodology can be also useful for decision makers who use different hydrological models. Indeed, if other calibrated hydrological models are used, even with higher residual uncertainty, the outcomes of the hydrological dam safety assessment study are expected to be similar, as the uncertainty assessment provides results close to the observations.

Lastly, the results of the impact of climate change on hydrological dam safety can vary when a different set of climate projections is used. In this study, most of the GCMs/RCMs considered point to increasing risk for the Eugui Dam in RCP 8.5, especially at the end of the century. Therefore, the signal (increasing risk in the future) seems to be consistent regardless of the climate models that are considered, although the magnitude of the changes could depend on the climate model and the projections considered. In this study, climate projections from the Coupled Model Intercomparison Project Phase 5 (CMIP5) were considered, as they are already downscaled by the EURO-CORDEX Program to a small spatial scale (0.11° grid spacing) which is suitable for impact assessment studies on a small river basin. Currently, CMIP5 climate projections have higher spatial resolution than CMIP6 projections do. We recommend the future development and use of the CMIP6 climate projections when available with finer a spatial scale to assess whether the results are sensitive to the climate projections used as input data.

## 6 Conclusions

A methodology to assess the impact of climate change on hydrological dam safety has been presented. Two hydrological models were used with climate projections supplied by an ensemble of 12 climate models as input data. The HBV continuous hydrological model was used to assess the impact of climate change on the reservoir water level frequency that supplies information about the expected initial reservoir water level in the future. The distributed and event-based RIBS hydrological model was used to transform the delta changes in precipitation quantiles

expected in the future into delta changes in peak flow quantiles. Moreover, all the sources of uncertainty in the methodology were assessed and incorporated to obtain sounder results that can increase the reliability of the conclusions.

The results show how climate change will have an impact on the initial water level expected at the beginning of flood events in the future, as well as on expected inflow peak discharges, reducing the hydrological dam safety. Indeed, the greatest expected changes in the maximum reservoir water levels will be expected at the end of the century in the scenario with higher emissions (RCP 8.5). At the same time, the results show how reducing emissions around 2040 (RCP 4.5) could lead to greater hydrological dam safety in the future. A warmer climate will lead to a decrease in the initial water levels in the reservoir, increasing the flood routing capacity of the dam to reduce outflow peaks, although with possible impacts on water management or energy production. Nonetheless, since the overtopping probability will in any case increase at the end of the century in RCP 8.5, dam managers will have to adapt strategies to optimize the water resource management in that scenario, lowering the reservoir water levels to face an increased risk with further implications for the water resources. The expected changes in maximum reservoir water levels in flood events will lead to changes in maximum outflow discharges. Therefore, regional and local civil protection bodies will need to adapt their current emergency plans for downstream of dams to new climate change scenarios. Indeed, local municipalities could consider the expected potential changes in outflow discharges released by upstream dams in their urban plans and potential mitigation measures to reduce flood risk, improving flood resilience in urban areas.

The stochastic procedure presented in this study incorporates the main sources of uncertainty and shows it is crucial in a hydrological dam safety analysis. Indeed, underestimates in maximum water levels and overtopping probabilities are obtained when the uncertainty is not included in the analysis. The results of this study are focused on the Eugui Dam, thus the conclusions cannot be extended to other dams. However, the methodology proposed can fulfil the requirements of recent dam regulations that demand the inclusion of climate projections in hydrological dam risk assessment analyses, such as the latest Spanish regulation about dam safety (BOE, 2021).

## Acknowledgements

The authors acknowledge the EURO-CORDEX Program for sharing their dataset and Carlos Garijo for his previous analysis and for allowing us to carry out this study. The authors acknowledge the Instituto Geográfico Nacional (IGN) for supplying the DTM, the SAIH real-time system of the River Ebro Basin Authority for supplying the sub-daily streamflow data, and the Centre for Hydrographic Studies of CEDEX for supplying the daily streamflow data.

## Disclosure statement

No potential conflict of interest was reported by the author(s).

## Funding

The authors acknowledge funding from the project PID2019-107027RB-I00 'SAFERDAMS: Assessment of the impact of climate change on hydrological dam safety' of the Agencia Estatal de Investigación of the Spanish Ministry of Science and Innovation (PID2019-107027RB-I00 / AEI / 10.13039/501100011033).

## ORCID

Marco Lompi  <http://orcid.org/0000-0003-2970-168X>  
Luis Mediero  <http://orcid.org/0000-0002-9346-6592>  
Enrique Soriano  <http://orcid.org/0000-0003-2764-6138>  
Enrica Caporali  <http://orcid.org/0000-0001-6389-3801>

## References

- Ahmadisharaf, E., *et al.*, 2016. A probabilistic framework for comparison of dam breach parameters and outflow hydrograph generated by different empirical prediction methods. *Environmental Modelling and Software*, 86, 248–263. doi:10.1016/j.envsoft.2016.09.022
- Ahmadisharaf, E. and Kalyanapu, A.J., 2015. Investigation of the impact of streamflow temporal variation on dam overtopping risk: case study of a high-hazard dam. *In: Proceedings of the World Environmental and Water Resources Congress*, 17–21 May 2015. Austin, TX, USA, 1050–1057.
- Alfieri, L., *et al.*, 2015. Global warming increases the frequency of river floods in Europe. *Hydrology and Earth System Sciences*, 19 (5), 2247–2260. doi:10.5194/hess-19-2247-2015
- Babur, M., *et al.*, 2016. Assessment of climate change impact on reservoir inflows using multi climate-models under Rcps - the case of Mangla Dam in Pakistan. *Water (Switzerland)*, 8 (9), 389. doi:10.3390/w8090389
- Bahls, V. and Holman, K., 2014. Climate change in hydrologic hazard analyses: Friant Dam Pilot Study - part I: hydrometeorological model inputs, Tech. rep., U.S. Department of the Interior, Bureau of Reclamation.
- Bergström, S., 1976. Development and application of a conceptual runoff model for Scandinavian catchments, SMHI Norrköping, Report RH07.
- Bergström, S., 1992. The HBV-model — Its structure and applications. SMHI Reports RH No. 4, Norrköping.
- Bezák, N., Brilly, M., and Šraj, M., 2014. Comparison between the peaks-over-threshold method and the annual maximum method for flood frequency analysis. *Hydrological Sciences Journal*, 59 (5), 959–977. doi:10.1080/02626667.2013.831174
- Blöschl, G., *et al.*, 2019. Changing climate both increases and decreases European river floods. *Nature*, 573 (7772), 108–111. doi:10.1038/s41586-019-1495-6
- BOE, 2021. Real Decreto 264/2021, de 13 de abril, por el que se aprueban las normas técnicas de seguridad para las presas y sus embalses. *Boletín Oficial del Estado*, 89 (Sec. I), 42480.
- Bowles, D., *et al.*, 2013. Guide to risk assessment for reservoir safety management, Guide, Tech. Rep. SC090001/R1, Environment Agency, Horison House, Deanery Road, Bristol, BS1 9AH.
- Brunner, M.I., *et al.*, 2019. Future trends in the interdependence between flood peaks and volumes: hydro-climatological drivers and uncertainty. *Water Resources Research*, 55 (6), 4745–4759. doi:10.1029/2019WR024701
- Brunner, M.I., *et al.*, 2018. Bivariate analysis of floods in climate impact assessments. *The Science of the Total Environment*, 616, 1392–1403. doi:10.1016/j.scitotenv.2017.10.176
- Bucak, T., *et al.*, 2017. Future water availability in the largest freshwater Mediterranean lake is at great risk as evidenced from simulations with the SWAT model. *Science of the Total Environment*, 582, 413–425. doi:10.1016/j.scitotenv.2016.12.149
- Cabral, M.C., *et al.*, 1992. A kinematic model of infiltration and runoff generation in layered and sloped soils. *Advances in Water Resources*, 15, 311–324. doi:10.1016/0309-1708(92)90017-V

- Chen, X. and Hossain, F., 2019. Understanding future safety of dams in a changing climate. *Bulletin of the American Meteorological Society*, 100 (8), 1395–1404. doi:10.1175/BAMS-D-17-0150.1
- Chernet, H.H., Alfredsen, K., and Midttømme, G.H., 2014. Safety of hydro-power dams in a changing climate. *Journal of Hydrologic Engineering*, 19 (3), 569–582. doi:10.1061/(ASCE)HE.1943-5584.0000836
- Costa, J.E., 1985. Floods from dam failures. *U.S. Geological Survey, Open-File Rep. No. 85-560*, Denver. p. 54
- Dankers, R. and Feyen, L., 2008. Climate change impact on flood hazard in Europe: an assessment based on high-resolution climate simulations. *Journal of Geophysical Research Atmospheres*, 113 (19), 1–17. doi:10.1029/2007JD009719
- Donat, M.G., et al., 2016. More extreme precipitation in the world's dry and wet regions. *Nature Climate Change*, 6 (5), 508–513. doi:10.1038/nclimate2941
- Doocy, S., et al., 2013. The human impact of floods: a historical review of events 1980–2009 and systematic literature review. *PLOS Currents Disasters*, 16, 1. doi:10.1371/currents.dis.f4deb457904936b07c09daa98ee8171a
- Fluixá-Sanmartín, J., et al., 2018. Review article: climate change impacts on dam safety. *Natural Hazards and Earth System Science*, 18 (9), 2471–2488. doi:10.5194/nhess-18-2471-2018
- Fluixá-Sanmartín, J., et al., 2019a. Empirical tool for the assessment of annual overtopping probabilities of dams. *Journal of Water Resources Planning and Management*, 145 (1), 1–12. doi:10.1061/(ASCE)WR.1943-5452.0001017
- Fluixá-Sanmartín, J., et al., 2019b. Quantification of climate change impact on dam failure risk under hydrological scenarios: a case study from a Spanish dam. *Natural Hazards and Earth System Science*, 19 (10), 2117–2139. doi:10.5194/nhess-19-2117-2019
- Fluixá-Sanmartín, J. et al., 2021. Accounting for Climate Change Uncertainty in Long-Term Dam Risk Management. *Journal of Water Resources Planning and Management*, 147, 04021012. doi:10.1061/(ASCE)WR.1943-5452.0001355
- Froehlich, D.C., 2008. Embankment dam parameters and their uncertainties. *Journal of Hydraulic Engineering*, 134 (12), 1708–1721. doi:10.1061/(ASCE)0733-9429(2008)134:12(1708)
- Garijo, C. and Mediero, L., 2019. Assessment of changes in annual maximum precipitations in the Iberian Peninsula under climate change. *Water (Switzerland)*, 11 (11). doi:10.3390/w11112375
- Garrote, L. and Bras, R.L., 1995a. A distributed model for real time forecasting using digital elevation models. *Journal of Hydrology*, 167 (1–4), 279–306. doi:10.1016/0022-1694(94)02592-Y
- Garrote, L. and Bras, R.L., 1995b. An integrated software environment for real-time use of a distributed hydrologic model. *Journal of Hydrology*, 167 (1–4), 307–326. doi:10.1016/0022-1694(94)02593-Z
- Girón, F., 1988. *The evacuation of floods during the operation of reservoirs*. San Francisco: Commission Internationale des Grands Barrages, Q.63-R.85, 1261–1283.
- Hargreaves, G.H., 1981. *Responding to tropical climates' The 1980–81 food and climate review*. Boulder, Colorado: The Food and Climate Forum, Aspen Institute for Humanistic Studies, 29–32.
- Hargreaves, G.H. and Samani, Z.A., 1985. Reference crop evapotranspiration from temperature. *Applied Engineering in Agriculture*, 1 (2), 96–99. doi:10.13031/2013.26773
- Hirabayashi, Y., et al., 2013. Global flood risk under climate change. *Nature Climate Change*, 3 (9), 816–821. doi:10.1038/nclimate1911
- Iglesias, A., et al., 2007. Challenges to manage the risk of water scarcity and climate change in the Mediterranean. *Water Resources Management*, 21 (5), 775–788. doi:10.1007/s11269-006-9111-6
- IPCC, 2012. Glossary of terms, in: managing the risks of extreme events and disasters to advance climate change adaptation. In: C. Field, et al., eds. *A special report of working groups I and II of the Intergovernmental Panel on Climate Change (IPCC)*. Cambridge, UK, New York, NY, USA: Cambridge University Press, 555–564.
- IPCC, 2014. Impacts, adaptation, and vulnerability, part a: global and sectoral aspects, contribution of working group II to the fifth assessment report of the intergovernmental panel on climate change, Cambridge University of Press, Cambridge, UK, New York, NY, USA, 20.
- Jacob, D., et al., 2020. Regional climate downscaling over Europe: perspectives from the EURO-CORDEX community. *Regional Environmental Change*, 20 (51). doi:10.1007/s10113-020-01606-9
- Jandora, J., et al., 2008. *The failure of embankment dams due to overtopping*. Brno, Czechia: VUTIUM.
- Jiménez-Álvarez, A., et al., 2013. Bases metodológicas del mapa de caudales máximos de las cuencas intercomunitarias, Centro de Estudios y Experimentación de Obras Públicas, Madrid, Spain, 96 (In Spanish).
- Katz, R.W., 2002. Techniques for estimating uncertainty in climate change scenarios and impact studies. *Climate Research*, 20 (2), 167–185. doi:10.3354/cr020167
- Kim, J., et al., 2013. Impacts of changes in climate and land use/land cover under IPCC RCP scenarios on streamflow in the Hoeya River Basin, Korea. *Science of the Total Environment*, 452–453, 181–195. doi:10.1016/j.scitotenv.2013.02.005
- Konapala, G., et al., 2020. Climate change will affect global water availability through compounding changes in seasonal precipitation and evaporation. *Nature Communications*, 11 (3044). doi:10.1038/s41467-020-16757-w
- Kundzewicz, Z.W., et al., 2017. Differences in flood hazard projections in Europe—their causes and consequences for decision making. *Hydrological Sciences Journal*, 62 (1), 1–14. doi:10.1080/02626667.2016.1241398
- Lee, B. and You, G.J., 2013. An assessment of long-term overtopping risk and optimal termination time of dam under climate change. *Journal of Environmental Management*, 121, 57–71. doi:10.1016/j.jenvman.2013.02.025
- Li, C., et al., 2019. Larger increases in more extreme local precipitation events as climate warms. *Geophysical Research Letters*, 46 (12), 6885–6891. doi:10.1029/2019GL082908
- Lompi, M., et al., 2021. Future flood hazard assessment for the city of Pamplona (Spain) Using an ensemble of climate change projections. *Water (Switzerland)*, 13, 792.
- Mallakpour, I., AghaKouchak, A., and Sadegh, M., 2019. Climate-induced changes in the risk of hydrological failure of major dams in California. *Geophysical Research Letters*, 46 (4), 2130–2139. doi:10.1029/2018GL081888
- Marahatta, S., et al., 2021. Application of SWAT in hydrological simulation of complex Mountainous River Basin (Part II: climate change impact assessment). *Water (Switzerland)*, 13 (1548). doi:10.3390/w13111548
- Matott, L.S., Babendreier, J.E., and Purucker, S.T., 2009. Evaluating uncertainty in integrated environmental models: a review of concepts and tools. *Water Resources Research*, 45 (W06421). doi:10.1029/2008WR007301
- Mediero, L., Garrote, L., and Martín-Carrasco, F.J., 2011. Probabilistic calibration of a distributed hydrological model for flood forecasting. *Hydrological Sciences Journal*, 56 (7), 1129–1149. doi:10.1080/02626667.2011.610322
- Meinshausen, M., et al., 2011. The RCP greenhouse gas concentrations and their extensions from 1765 to 2300. *Climatic Change*, 109 (1), 213–241. doi:10.1007/s10584-011-0156-z
- Michailidi, E.M. and Bacchi, B., 2017. Dealing with uncertainty in the probability of overtopping of a flood mitigation dam. *Hydrology and Earth System Sciences*, 21 (5), 2497–2507. doi:10.5194/hess-21-2497-2017
- Monteith, J.L., 1965. Evaporation and environment. *Symposia of the Society for Experimental Biology*, 19, 205–224.
- Morales-Torres, A., et al., 2016. The suitability of risk reduction indicators to inform dam safety management. *Structure and Infrastructure Engineering*, 12, 1465–1476. doi:10.1080/15732479.2015.1136830
- Moriasi, D.N., et al., 2015. Hydrologic and water quality models: performance measures and evaluation criteria. *Transactions of the American Society of Agricultural and Biological Engineers*, 58, 1763–1785. doi:10.13031/trans.58.10715
- Myhre, G., et al., 2019. Frequency of extreme precipitation increases extensively with event rareness under global warming. *Scientific Reports*, 9 (16063), 1–10. doi:10.1038/s41598-019-52277-4

- Najibi, N. and Devineni, N., 2018. Recent trends in the frequency and duration of global floods. *Earth System Dynamics*, 9 (2), 757–783. doi:10.5194/esd-9-757-2018
- Nash, J.E. and Sutcliffe, J.V., 1970. River flow forecasting through conceptual models part I—A discussion of principles. *Journal of Hydrology*, 10 (3), 282–290. doi:10.1016/0022-1694(70)90255-6
- Nilawar, A.P. and Waikar, M.L., 2019. Impacts of climate change on stream flow and sediment concentration under RCP 4.5 and 8.5: a case study in Purna river basin, India. *Science of the Total Environment*, 650, 2685–2696. doi:10.1016/j.scitotenv.2018.09.334
- Novembre, N., et al., 2015. Climate change in hydrologic hazard analyses: Friant Dam Pilot Study – part II: using the SEFM with climate-adjusted hydrometeorological inputs, Technical Memorandum 8250-2015-010, U.S. Department of the Interior, Bureau of Reclamation.
- Oubennaceur, K., et al., 2021. Flood risk assessment under climate change: the Petite Nation River Watershed. *Climate*, 9 (125), 125. doi:10.3390/cli9080125
- Pastor, A.V., et al., 2014. Accounting for environmental flow requirements in global water assessment. *Hydrology and Earth System Sciences*, 18 (12), 5041–5059. doi:10.5194/hess-18-5041-2014
- Peter, S., et al., 2018. Development of probabilistic dam breach model using Bayesian inference. *Water Resources Research*, *American Geophysical Union*, 54 (7), 4376–4400. doi:10.1029/2017wr021176ff
- Prudhomme, C. and Davies, H., 2009. Assessing uncertainties in climate change impact analyses on the river flow regimes in the UK. Part 2: future climate. *Climatic Change*, 93 (1–2), 197–222. doi:10.1007/s10584-008-9461-6
- Quintero, F., et al., 2018. Assessment of changes in flood frequency due to the effects of climate change: implications for engineering design. *Hydrology*, 5 (19), 19. doi:10.3390/hydrology5010019
- Refsgaard, J.C., et al., 2007. Uncertainty in the environmental modelling process - A framework and guidance. *Environmental Modelling and Software*, 22 (11), 1543–1556. doi:10.1016/j.envsoft.2007.02.004
- Riahi, K., et al., 2011. RCP 8.5 — A scenario of comparatively high greenhouse gas emissions. *Climatic Change*, 109 (1–2), 33–57. doi:10.1007/s10584-011-0149-y
- Rojas, R., et al., 2012. Assessment of future flood hazard in Europe using a large ensemble of bias-corrected regional climate simulations. *Journal of Geophysical Research Atmospheres*, 117. doi:10.1029/2012JD017461
- Roudier, P., et al., 2016. Projections of future floods and hydrological droughts in Europe under a +2°C global warming. *Climatic Change*, 135 (2), 341–355. doi:10.1007/s10584-015-1570-4
- Seibert, J. and Vis, M.J.P., 2012. Teaching hydrological modeling with a user-friendly catchment-runoff-model software package. *Hydrology and Earth System Sciences*, 16 (9), 3315–3325. doi:10.5194/hess-16-3315-2012
- Stevenson, T., Townson, J.M., and Wilson, W.M., 1981. The Stevenson formula for predicting wave height', Technical note. *Proceedings of the Institution of Civil Engineers*, 71 (3), 907–909. doi:10.1680/iicep.1981.1826
- Tarouilly, E. and Lettenmaier, D., 2021. Uncertainty in Probable Maximum Precipitation for Dam Safety. *EGU General Assembly Conference Abstracts*.
- Tennant, D.L., 1976. Instream flow regimens for fish, wildlife, recreation and related environmental resources. *Fisheries Magazine*, 1 (4), 6–10. doi:10.1577/1548-8446(1976)001<0006:IFRFFW>2.0.CO;2
- Thomson, A.M., et al., 2011. RCP 4.5: a pathway for stabilization of radiative forcing by 2100. *Climatic Change*, 109 (1–2), 77–94. doi:10.1007/s10584-011-0151-4
- USACE, 2016. *Guidance for incorporating climate change impacts to Inland hydrology in civil works studies, designs, and projects*. Washington, DC: United States Army Corps of Engineers, EBC, 2016–2025.
- Van Der Keur, P., et al., 2010. Identifying uncertainty guidelines for supporting policy making in water management illustrated for upper Guadiana and Rhine Basins identifying uncertainty guidelines for supporting policy making in water management illustrated for upper Guadiana and Rhine. *Water Resources Management*, 24 (14), 3901–3938. doi:10.1007/s11269-010-9640-x
- Wahl, T.L., 2004. Uncertainty of predictions of embankment dam breach parameters. *Journal of Hydraulic Engineering*, 130 (5), 389–397. doi:10.1061/(ASCE)0733-9429(2004)130:5(389)
- Winsemius, H.C., et al., 2015. Global drivers of future river flood risk. *Nature Climate Change*, 6 (4), 381–385. doi:10.1038/nclimate2893
- Woolway, R.I., et al., 2020. Global lake responses to climate change. *Nature Reviews Earth & Environment*, 1 (8), 388–403. doi:10.1038/s43017-020-0067-5
- Yu, L., et al., 2021. Multi-objective optimal operation of cascade hydropower plants considering ecological flow under different ecological conditions. *Journal of Hydrology*, 601 (126599), 126599. doi:10.1016/j.jhydrol.2021.126599